Memoirs of the Faculty of Engineering, Nagoya University
Vol. 39, No. 1 (1987)

PRINCIPLES OF METALLURGICAL REACTION ENGINEERING

IWAO MUCHI, SHIGEO ASAI and MAMORU KUWABARA

Department of Metallurgy and Iron and Steel Engineering

(Received May 29, 1987)

Abstract

The studies of the simulation of metallurgical processes have been developed over the past decade, and this rapid development has rendered the service to realize the available techniques for solving practical problems in process metallurgy.

"Metallurgical Reaction Engineering" implies the academic subject in the field of engineering, relevant to reaction or reactor in the field of process metallurgy. Now, it has become an essential subject in metallurgical engineering, and its methodology is used in the practice of metallurgical process development. Obviously, this small article cannot cover all the topics which are concerned with the metallurgical reactions and transport processes.

This article primarily provides a rational and rigorous approach on the basis of the mathematical expressions for the important phenomena occurring in metallurgical processes, and the mathematical modelings of both lumped and distributed systems are presented.

This article is organized into two main parts: Part 1 is concerned with the topics in ironmaking processes and Part 2 includes those in steelmaking processes. Each part provides the methodology of metallurgical reaction engineering, beginning with the fundamental principles and continuing to the practical applications.

CONTENTS

1. Preface

A mathematical model is useful for the successful design and operation of metallurgical processes and for the deeper understanding of the phenomena occuring in them.

This review is intended to present the fundamental procedure for building the mathematical model which should be developed to reach and grasp the essential facts without getting too much involved in the details of the phenomena.

Modelling procedures given in this review are primarily concerned with the application of both the theories of transport phenomena and the well-known principles of chemical reaction engineering. Thus, a new field which can be called as "metallurgical reaction engineering" is developed here, and its applications to some metallurgical plants are presented individually.

This review is divided into two parts. In Part 1, we deal with the modelling of the ironmaking processes, and Part 2 is concerned with the modelling of the steelmaking processes.

Most of ironmaking and steelmaking processes include a complex phenomena. Especially in blast furnace, a theoretical approach is obstructed due to the complicated reactions, the severe nonuniform temperature distribution and also the lack of practical and reliable data.

In general, since the metallurgical operations are conducted at relatively high temperatures, mass transfer may mostly play an important role in determining the rate of overall reaction, where the mixing phenomena become a crucial problem. Particularly, in steelmaking processes, the kinetics of many reactions can be con-

trolled by mass transfer, and both the intensity of mixing and the temperature of melt affect the selectivity of the complex reaction, for instance, the preferential oxidation of silicon in comparison with decarburization as in LD converter.

This review cannot cover all the existing ironmaking and steelmaking processes. Lack of space forbids us to discuss about the other furnaces which are running in metallurgical industry.

Finally, the authors would like to express their appreciation to Mr. Alireza Radjai who is a graduate student in Nagoya University for his help in editing of the manuscript and to Research Associate Mr. Kensuke Sassa for his efforts in typing the manuscript.

Part 1 Modelling of Ironmaking Processes

2. Basic Concepts in Modelling

2. 1. Vectorial Ergun's Equation

Pyrometallurgical processing of solid natural resources is frequently performed in the packed beds through which gas is flowing to promote the convective mass and heat transfer and the rate of the chemical processes involved. Therefore, flow structures in the beds strongly affect the performance of the processes.

Extensive investigations have been conducted to obtain the momentum transfer equation characterizing the flow dynamics in a porous media. Nevertheless, it is virtually intractable to solve the Navier-Stokes equation for the fluid flow in multiply connectd interparticle regions despite a few attempts[1,2] hitherto made. A preliminary, yet alternative approach to this problem was devoted to developing the "hydraulic" or "pipe-flow" equations for the one-dimensional flow of fluids through granular beds. Employing this type of approach, Kozeny-Carman equation[3] for laminar flow and Burke- Plummer equation[4] for turbulent flow were successfully derived making allowance for the mean hydraulic radius of the flow capillaries and for the effect of voidage. Ergun[5] comprehensively correlated these two equations by simply adding to yield an expression in the form:

$$\frac{\Delta P}{L}=\frac{150\mu_g u_g}{{d_p}^2}\frac{(1-\varepsilon)^2}{\varepsilon^3}+1.75\frac{\rho_g u_g^2}{d_p}\frac{(1-\varepsilon)}{\varepsilon^3} \tag{2.1}$$

where u_g is the superficial velocity and ρ_g is the density of the fluid at the arithmetic average of the end pressures. This additive characteristic of the viscous and kinetic pressure loss terms has been confirmed theoretically from the Navier-Stokes equation by Irmay[6].

A transformation of the Ergun equation is represented in dimensionless groups of Blake as:

$$\frac{\rho_g \Delta P}{G_g^2}\left(\frac{d_p}{L}\right)\left(\frac{\varepsilon^3}{1-\varepsilon}\right)=150\frac{1-\varepsilon}{Re_p}+1.75 \tag{2.2}$$

where $G_g(=\rho_g u_g)$ is the mass velocity and $Re_p(=d_p G_g/\mu_g)$ refers to the Reynolds

number.

One should by careful here that the particle size d_p in the Ergun equation is defined in terms of the specific surface area of a unit volume of solid particles S_v as:

$$d_p=6/S_v \tag{2.3}$$

That is to say, d_p denotes the diameter of equivalent spheres having the same specific surface area as the non-spherical packing employed. For dispersed beds with a wide range of particle size, it is necessary to calculate a representative mean diameter. For the multiply-sized packings with the representative diameters d_{pi} ($i=1$ to k), an expression of average specific surface area consequently allows to give the average particle size in the form:

$$d_p=1/\sum_{i=1}^{k}(n_i/d_{pi}) \tag{2.4}$$

where n_i stands for the fractional volume of the i-th classified size-segment.

It should be noted furthermore that several investigators[7~9] have critically evaluated the Ergun equation without producing consistent viscous and inertia tortuosity constants. However, the scatter of data has been attributed not to the Ergun type expression but rather to the influences of packing shape, orientation, voidage, entrance effects and excess voidage at the walls [8~10].

The study of pressure loss in the moving bed has recently become an interesting subject for solid processing. Yoon and Kunii[11] have confirmed that the Ergun equation for the fixed bed system is well applicable also to the moving bed system, provided a slip velocity of the fluid relative to the descending solid particles is used instead of the superficial fluid velocity in fixed beds as well as taking the variation of voidage with the gas velocity[12] or with the desceending velocity of solid particles[13~15] into consideration.

Special attention should be paid to the nonuniform flows associated with the voidage and particle size variations in beds. We are particularly concerned with those aspects which are relevant to the blast furnace operation. The proper approach to the problem can be accomplished by using the equation of continuity as well as the Ergun equation in their vectorial forms[16,17]. When the gas evolution is relatively negligible, the set of the governing equations are as follows:

$$\mathrm{div}\,\vec{G}_g=0 \tag{2.5}$$

$$\mathrm{grad}\,P=-(f_1+f_2|\vec{G}_g|)\vec{G}_g \tag{2.6}$$

$$f_1\equiv 150(1-\varepsilon)^2\mu_g/\rho_g(\phi d_p)^2\varepsilon^3,$$

$$f_2\equiv 1.75(1-\varepsilon)/\rho_g(\phi d_p)\varepsilon^3 \tag{2.7}$$

where $\vec{G}_g$ is the mass velocity vector and f's stand for the Ergun's coefficients of resistance.

Subsequent to the preliminary application[17~19] to the idealized simple systems, this set of equations has been applied to the blast furnace system with more complicated numerical techniques originally by Radestock and Jeschar[16], Szekely et

al.[20~22] and Kuwabara and Muchi[23~25], resulting in a great amount of information on the behavior of nonuniform flows through the layered configuration of burdens.

We now proceed to describe the way to solve Eqs. (2.5) and (2.6) for the fluid flow through two-dimensional or axi-symmetrical beds having spatially variable resistances. The equation of continuity given by Eq. (2.5) can be satisfied by working in terms of the stream function ψ which is defined as:

$$G_{gr}=r^{-m}(\partial\psi/\partial z) \tag{2.8}$$

$$G_{gz}=-r^{-m}(\partial\psi/\partial r) \tag{2.9}$$

where $m=0$ for two-dimensional flow and $m=1$ for axi-symmetrical flow. Thus, if the terms involving velocity are displaced by the stream function, there will be no need to make any explicit expression of the mass-conservation principle.

The directional components of the Ergun equation, Eq. (2.6), can be written as:

$$\partial P/\partial r=-(f_1+f_2|\vec{G}_g|)G_{gr} \tag{2.10}$$

$$\partial P/\partial z=-(f_1+f_2|\vec{G}_g|)G_{gz} \tag{2.11}$$

Gas pressure P can be entirely removed from Eqs. (2.10) and (2.11) by using a mathematical relationship described as:

$$\partial^2 P/\partial r\partial z=\partial^2 P/\partial z\partial r \tag{2.12}$$

The resultant equation in terms of the stream function ψ is as follows:

$$\left\{\frac{\partial f_1}{\partial r}\frac{\partial\psi}{\partial r}+\frac{\partial f_1}{\partial z}\frac{\partial\psi}{\partial z}+f_1\left(\frac{\partial^2\psi}{\partial r^2}+\frac{\partial^2\psi}{\partial z^2}-\frac{m}{r}\frac{\partial\psi}{\partial r}\right)\right\}\sqrt{\left(\frac{\partial\psi}{\partial r}\right)^2+\left(\frac{\partial\psi}{\partial z}\right)^2}$$
$$+\frac{1}{r^m}\left\{\frac{\partial f_2}{\partial r}\frac{\partial\psi}{\partial r}+\frac{\partial f_2}{\partial z}\frac{\partial\psi}{\partial z}+f_2\left(\frac{\partial^2\psi}{\partial r^2}+\frac{\partial^2\psi}{\partial z^2}-\frac{m}{r}\frac{\partial\psi}{\partial r}\right)\right\}\left\{\left(\frac{\partial\psi}{\partial r}\right)^2\right.$$
$$\left.+\left(\frac{\partial\psi}{\partial z}\right)^2\right\}+\frac{f_2}{r^m}\left\{\left(\frac{\partial\psi}{\partial r}\right)^2\left(\frac{\partial^2\psi}{\partial r^2}-\frac{m}{r}\frac{\partial\psi}{\partial r}\right)+\left(\frac{\partial\psi}{\partial z}\right)^2\left(\frac{\partial^2\psi}{\partial z^2}-\frac{m}{r}\frac{\partial\psi}{\partial r}\right)\right.$$
$$\left.+2\left(\frac{\partial\psi}{\partial r}\frac{\partial\psi}{\partial z}\right)\frac{\partial^2\psi}{\partial r\partial z}\right\}=0 \tag{2.13}$$

Equation (2.13) in a finite-difference form, together with the appropriate boundary conditions, gives the value for ψ at any point in the field, provided the spatially distributed flow resistance has been specified. Once the solution for ψ has been obtained, velocity can be evaluated by Eqs. (2.8) and (2.9). Pressure recovers basically through the appropriate integration of Eqs. (2.10) and (2.11). However, the following numerical scheme may be advantageously applied to avoid the accompanying integration error. That is, the divergence of Eq. (2.6), combined with Eq. (2.5), yields:

$$\Delta P=\frac{\partial^2 P}{\partial z^2}+\frac{1}{r^m}\frac{\partial}{\partial r}\left(r^m\frac{\partial P}{\partial r}\right)=-G_{gr}\frac{\partial W}{\partial r}-G_{gz}\frac{\partial W}{\partial z} \tag{2.14}$$

where

$$W\equiv f_1+f_2|\vec{G}_g| \tag{2.15}$$

The iterative solution of Eq. (2. 14) also gives the pressure at all points in the furnace. During the course of the solution for ψ, we usually need to know the pressure and the temperature because their variations may affect gas density which in turn requires recasting of the flow resistance.

Photograph 2. 1 shows the experimentally observed streamlines of nitrogen gas

(a)

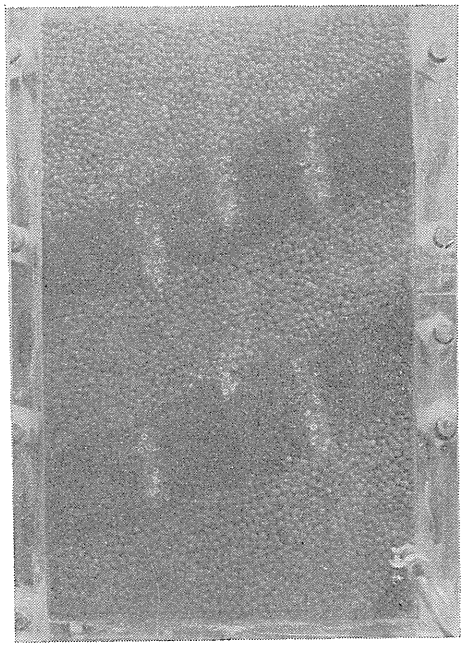

(b)

Photo. 2. 1. Visualized gas-streamlines in packed bed.

(a) Gas-streamlines near the top surface.

(b) Gas streamlines in the layered structure of burdens.

flowing through a two-dimensional rectangular bed ($200\times15\times660$ mm^3) packed with silica-gel particles. Auxiliary flow of steam injected from six injectors attached to the back of the bed allowed to visualize the streamlines. In Photo. 2.1-(a), we can find the centralized flow near the inclined top surface of the bed. Photograph 2.1-(b) shows the zigzag flow regime in the layered structure of burdens, where the particle diameters in the bright and dark layers were 4.4 mm and 2.6 mm, respectively. These gas flow-patterns, basically simulating the gas-flow through the shaft of the blast furnace, can be also predicted based on the numerical scheme described in this section.

2. 2. Estimation of Reactor Model Parameters

In order that a mathematical process model can be completely specified, we need the transport and thermodynamic properties which must supplement the governing equation. Some representative relations wlll be given here.

(1) Dispersion Coefficient of Fluid (D_{jn})

As for fluid flow in porous media, dispersion of mass stems from hydrodynamic fluctuation of fluid velocity rather than molecular diffusion and can be evaluated on the basis of the empirical relationship[26] between Péclet number Pe_{jn} ($=d_pV_{jz}/D_{jn}$) and particle Reynolds number Re_{pj}, where V_{jz} designates the axial linear velocity of fluid. Over the Re_{pj} range greater than about 100, Pe_{jn} normally takes the following constant values:

$$Pe_{gr}=10,\ Pe_{gz}=2,\ Pe_{lr}=50,\ Pe_{lz}=0.5 \tag{2.16}$$

whereas in the low Re_{pj} range, the Pe_j, regardless of the flow direction, increases linearly with the increase in Re_{pj} according to a constant Schmidt number ($\mathrm{Sc}=\mu_g/\rho_gD_j$).

(2) Effective Thermal Conductivity of Fluid (K_{jn})

For the turbulent regime likely in the ordinary solid-processing, the same magnitude of thermal diffusion as of mass diffusion may prevail, and we have the following relation:

$$Pe_{jn}=d_pV_{jz}/(K_{jn}/c_j\rho_j),\quad (j=g,\ l\ ;\ n=r,\ z) \tag{2.17}$$

(3) Effective Thermal Conductivity of Burden (K_b)

Since the solid-solid thermal conduction through the point of contact is relatively small, K_b is governed by the indirect and direct radiation whose mechanism was formulated by Shotte[24] as follows:

$$K_b=(1-\varepsilon)/(1/k_s+1/k_r)+\varepsilon k_r,$$
$$k_r=2.29\times10^{-7}d_p(T_s)^3\ [\mathrm{W/m\cdot K}] \tag{2.18}$$

(4) Interphase Heat Transfer Coefficient (h_p)

When we define the parameter, h_p, based on a mean temperature of solid particles with and without the surrounding melt, h_p should be an overall parameter involving the true gas/burden film heat transfer coefficient (h_p') and the burden conductivity (k_s). The expression for spheres was given by Stuke[28] in the form:

$$h_p/h_p'=1/(1+Bi/10) \tag{2.19}$$

where $Bi=h_p' d_p/k_s$ stands for Biot number. Thermal conductivity of solid takes the values of about 0.58 W/m·K for coke and 1.63 W/m·K for ore materials[29].

True heat transfer coefficient h_p' can be estimated by the empirical relationship for the Nusselt number ($Nu=h_p' d_p/k_g$), where k_g is the thermal conductivity of the fluid. Heat transfer around a single sphere is well correlated according to the Ranz and Marshall's equation[30] represented by:

$$Nu=2.0+0.6(Pr)^{\frac{1}{3}}(Re_p)^{\frac{1}{2}} \tag{2.20}$$

where $Pr(=c_g\mu_g/k_g)$ is the Prandtl number.

For the packed granular beds where interparticle jets impinge against the downstream particles, Eq. (2.20) with the Reynolds number multiplied by a factor $n(=9$ to $10)$ may be also working[31]. Shirai[32] has proposed an alternative correlation which allows to evaluate the effect of the voidage(ε) as follows:

$$\varepsilon Nu=2.0+0.75(Pr)^{\frac{1}{3}}(Re_p)^{\frac{1}{2}} \tag{2.21}$$

(5) Mass Transfer Coefficient (k_f)

Based on the similarity between the heat and the mass transfer phenomena, the preceding relationships for the heat transfer coefficient, h_p', may be available in similar forms provided the Nusselt number and the Prandtl number are replaced by the Sherwood number ($Sh=k_f d_p/D_j$) and the Schmidt number, respectively.

(6) Specific Heat of Gas/Burden (c_j)

Specific heas of multicomponent gas or burden can be evaluated by:

$$c_j=\sum_{i=1}^{n}(C_i)_j M_i c_i/\sum_{i=1}^{n}(C_i)_j M_i \quad (j=g,\ b) \tag{2.22}$$

where c_i is the specific heat of each component i and is expressed as a function of temperature , and C denotes the molar concentration.

Nomenclature

Bi : Biot number (−)
C : molar concentration (kmol/m³)
c : specific heat (J/kg·K)
D : dispersion coefficient (m²/s)
d_p : particle diameter (m)
f_1, f_2 : Ergun's coefficient of resistance (1/s), (m²/kg)
G : mass velocity (kg/m²·s)
h_p : heat transfer coefficient between gas and solid particles (W/m²·K)
K : effective thermal conductivity (W/m·K)
k : thermal conductivity (W/m·K)
k_f : mass transfer coefficient (m/s)
L : bed height (m)
M : molecular mass (kg/kmol)
Nu : Nusselt number (−)

P : gas pressure (Pa)
ΔP : pressure loss (Pa)
Pe : Péclet number for mass transfer (−)
Pr : Prandtl number (−)
Re_p : particle Reynolds number (−)
r : radial distance (m)
Sc : Schmidt number (−)
Sh : Sherwood number (−)
S_v : specific surface area (m^2/m^3)
T : temperature (K)
u : superficial velocity (m/s)
V : linear velocity (m/s)
z : axial distance (m)
ε : voidage (−)
μ : viscosity (Pa·s)
ρ : density (kg/m^3)
ϕ : shape factor of solid particle (−)
ψ : stream function ($m=0$: kg/m·s, $m=1$: kg/s)
(Subscripts)
b : burden, g : gas, l : liquid, r : radial direction, s : solid particle, z : axial direction

References

1) Sareen, S. S., Ph D Dissertation, Chap. VI, Illinois Institute of Technology, (1970).
2) Stark, K. P., "Fundamentals of Transport Phenomena in Porous Media", 86, Elsevier, (1972).
3) Carman, P. C., Trans. Inst. Chem. Engrs., 15, 150 (1937).
4) Burke, S. P. and Plummer, W. B., Ind. Eng. Chem., 20, 1196 (1928).
5) Ergun, S., Chem. Eng. Progr., 48, 89 (1952).
6) Irmay, S., Trans. Am. Geophys. Union, 39, 702 (1958).
7) Wentz, C. A. and Thodas G., A. I. C*h*. E. Journal, 9, 81 (1963).
8) Smith, K. L. and Roper, G. H., Australian Chem. Eng., 4, 5 (1960).
9) Handley, D. and Heggs, P. J., Trans. Inst. Chem. Eng. (London), 46, T251 (1968).
10) Mehta, D. and Hawley, M. C., Ind. Eng. Chem., Process Design and Develop., 8, 280 (1969).
11) Yoon, S. m. and Kunii, D., Ind. Eng. Chem., Process Design and Develop., 9, 559 (1970).
12) Sissom, L. E. and Jackson, T. W., J. Heat Transfer, Trans. ASME, 89, 1 (1967).
13) Ernst, R., Chem. Ing. Tech., 32, 17 (1960).
14) Takahashi, H. and Yanai, H., Kagaku Kōgaku, 35, 357 (1971).
15) Shimizu, M., Yamaguchi, A., Inaba, S. and Narita, K., Tetsu-to-Hagané, 68, 936 (1982).
16) Radestock, J. and Jeschar, R., Stahl u. Eisen, 90, 1249 (1970).
17) Stanek, V. and Szekely, J., A. I. C*h*. E. Journal, 20, 974 (1974).
18) Stanek, V. and Szekely, J., Can. J. Chem. Eng., 50, 9 (1972).
19) Szekely, J. and Poveromo, J. J., A. I. C*h*. E. Journal, 21, 769 (1975).
20) Poveromo, J. J., Szekely, J. and Propster, M. A., "Proc. Blast Furnace Aerodynamic Symposium", ed. by Standish, N., 1, AIMM, Wollongong, (1975).
21) Szekely, J. and Propster, M. A., Trans. ISIJ, 19, 21 (1979).
22) Propster, M. A. and Szekely, J., Ironmaking & Steelmaking, 6, 209 (1979).

23) Kuwabara, M. and Muchi. I., "Proc. Blast Furnace Aerodynamic Symposium", ed. by Standish, N., 61, AIMM, Wollongong, (1975).
24) Kuwabara, M. and Muchi, I., Tetsu-to-Hagané, 62, 463 (1976).
25) Kuwabara, M. and Muchi, I., Trans. ISIJ, 17, 330 (1977).
26) Levenspiel. O, "Chemical Reaction Engineering", 275, John Wiley & Sons, (1962).
27) Shotte, W., A. I. C*h*. E. Journal, 6, 63 (1960).
28) Stuke, B., Angew. Chem., B20, 262 (1948).
29) Mertes, H., Dr. -Ing. -Diss., Techn. Univ. Clausthal, (1968).
30) Ranz, W. E. and Marshall, W. R., Chem. Eng. Progr., 48, 141 (1952).
31) Ranz, W. E., Chem. Eng. Progr., 48, 247 (1952).
32) Shirai. T., Kagaku Kōgaku-to-Kagaku Kikai, 1, 216 (1956).

3. Mathematical Descriptions for Ironmaking Processes

3. 1. Model for Prediction of Gas Temperature at the Top of Blast Furnace

Iron ore and coke are fed batchwise into the top of bed in blast furnace. Thus, during the descending of the burden, the temperatures of gas and burden at the top of bed change unsteadily. The information concerning variation in the temperature of top gas is used to control the actual operation.

One charge of burden is intermittently fed into the top of blast furnace. Now we designate the bed height of one charge as, z, which can be determined from the following expression:

$$z=\left\{\left(\frac{w_c}{\rho_c}\right)+\left(\frac{w_o}{\rho_o}\right)\right\}/A \tag{3.1}$$

where ρ_c and ρ_o are the bulk densities of coke and iron ore layers (kg/m^3 (bed)), respectively, w_c and w_o are the masses of coke and iron ore per one charge (kg/ch), respectively, and A is the cross sectional area of the top of furnace.

The bed of one charge descends gradually, and when the top level of the bed reaches to the height specified previously next charge is fed into the top of the bed.

Here we develop a simple model[1] to determine the temperatures of top gas at two different times, namely at the time just before the next charge is fed, T_Z, and at the time immediately after the charging is finished, T_0.

For simplicity, we assume that coke and iron ore have the same specific heats, temperatures and particle diameters. Furthermore, we assume that the surrounding surface of the blast furnace is made of adiabatic wall, and also we can neglect the heat of reaction.

By taking heat balance for gas around the differential bed height in one charge, Eq. (3.2) can be obtained.

$$\frac{dT}{dx}=\frac{\alpha}{WC}(T-t) \tag{3.2}$$

where T is gas temperature, x is distance from the top of bed, W is mass flow rate of gas (kg/s), C is specific heat of gas (J/kg·K), t is temeperature of solid particles. We refer to α(W/m·K) as $\alpha=6(1-\varepsilon)h_pA/d_p$, where ε is voidage, h_p is heat transfer coefficient between solid particle and gas, and d_p is diameter of solid

particle.

Similarly, Eq. (3.3) can be obtained by taking heat balance for solid particle around the same differential bed as mentioned above

$$\frac{dt}{dx}=\frac{\alpha}{wc}(T-t) \tag{3.3}$$

where w is mass flow rate of solid particles and c is specific heat of solid particle.

The values of W and w can be determined from the following equations. From the mass balance for nitrogen gas, we have

$$W=79F_b\rho/(\%N_2) \tag{3.4}$$

where F_b is blast volume (Nm^3/s), ρ is density of gas at the top of bed (kg/Nm^3) and $(\%N_2)$ is the mean concentration of N_2 in the gas exhausted from the top of bed, and

$$w=n(w_c+w_o) \tag{3.5}$$

where n is the number of charges per hour (ch/3600s). Now, we use the symbols $\beta\equiv\alpha/wc$, $\gamma\equiv wc/WC$ and $\delta\equiv\beta(1-\gamma)$. From Eqs. (3.2) and (3.3), we have the following equations.

$$dT=\gamma dt \tag{3.6}$$

$$d(T-t)/(T-t)=-\delta dx \tag{3.7}$$

Integrating Eq. (3.6) and Eq. (3.7), respectively, we have

$$T=\gamma t+C_1 \tag{3.8}$$

$$T-t=\exp(-\delta x+C_2)=B\exp(-\delta x) \tag{3.9}$$

where C_1 and C_2 are constants and $B\equiv\exp(C_2)$.

From Eqs. (3.8) and (3.9),

$$t=c_1\exp(-\delta x)+c_2 \tag{3.10}$$

$$T=c_1\gamma\exp(-\delta x)+c_2 \tag{3.11}$$

where $c_1\equiv B/(\gamma-1)$ and $c_2\equiv -C_1/(\gamma-1)$, In Eq. (3.11), we put $T\equiv T_z$ at $X=z$, and $T=T_0$ at $x=0$, thus

$$T_z=c_1\gamma\exp(-\delta z)+c_2 \tag{3.12}$$

$$T_0=c_1\gamma+c_2 \tag{3.13}$$

Furthermore, in Eq. (3.10), putting $t=t_0$ at $x=0$ we get

$$c_2=t_0-c_1 \tag{3.14}$$

where t_0 is the temperature of solid particles to be fed into the top of furnace. From Eqs. (3.12) and (3.14), we obtain

$$T_z=c_1\lambda+t_0 \tag{3.15}$$

where $\lambda \equiv \gamma \exp(-\delta z) - 1$. Now, the top gas temperature varies from T_z to T_0, and we designate the mean temperature T_m which can be expressed as Eq. (3.16).

$$T_m = \frac{1}{z}\int_0^z T\,dx = \frac{c_1\gamma}{\delta z}\{1-\exp(-\delta z)\} + c_2 \tag{3.16}$$

We substitute Eqs. (3.14) and (3.15) into Eq (3.16) to get

$$T_z = \{T_m + t_0(\nu - 1)\}/\nu \tag{3.17}$$

where $\nu \equiv [\gamma\{1-\exp(-\delta z)\} - \delta z]/\lambda\delta z$. Now, from Eqs. (3.15) and (3.17), we obtain

$$c_1 = (T_m - t_0)/\lambda\nu \tag{3.18}$$

When the data of A, ε, h_p, d_p, n, w_c, w_o, C, c, F_b, ($\%N_2$), ρ, ρ_c, ρ_o, and T_m are given, we can determine the values of c_1 and c_2 by Eq. (3.18) and Eq. (3.14), respectively. Thus, we can evaluate T_z and T_0 from Eq. (3.12) and Eq. (3.13), respectively.

Furthermore, if the supply of burden is suspended due to problems in the feeding machine during the time period, θ, but the blast is successively continued, then the temperature of top gas can be estimated from Eq. (3.19).

$$T = c_2 + c_1\gamma\exp(-\delta u_s\theta) \tag{3.19}$$

where $u_s = zn$ is the descending velocity of solid particles.

3. 2. Layered Structure Model of Blast Furnace

(I) Introduction

In the steady state operation of blast furnace, layered configuration of ore and coke burdens is accompanied by not only the longitudinal but also the radial variations of the process variables which would fluctuate periodically with the alternate passage of the layers. This section is devoted to describing such situations in blast furnace based on a mathematical model[2~3]. Fundamental notation for the physical and transport properties is the same as in section 2.

(II) Radial Distribution of Gas Flow Rate

The interrelation between a burden distribution associated with the charging arrangement and the resultant radial distribution of the gas flow rate is analytically formulated here. Assumptions made are as follows:

(i) As shown in Fig. 3. 1, the layered ore and coke burdens charged to the top of the furnace descend with V-shaped contours whose apparent angles of repose are α_1 and α_2, respectively.

(ii) When the two adjacent layers are

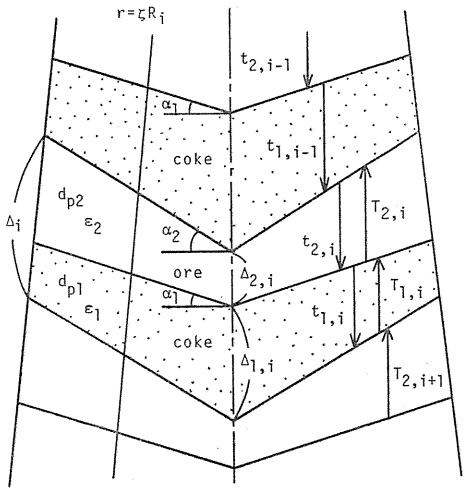

Fig. 3. 1. Schematic illustration of the layered structure model.

considered as one block, the i-th block is a cylindrically packed bed having an average diameter R_i, and the resistance to flow at a given dimensionless radial position ($\zeta=r/R_i$) is the same in any block.

(iii) Ore and coke burdens are prepared through sufficient screening, consequently resulting in no radial distribution of the particle size d_{pj} and the voidage ε_j in each layer.

The Ergun equation, making allowance for the radial distribution of the longitudinally averaged particle size $\bar{d}_p$ and the voidage $\bar{\varepsilon}$, takes the form:

$$\partial P/\partial z=\rho_g\{1-\bar{\varepsilon}(\zeta)\}\cdot\bar{\psi}(\zeta)\cdot u_g(\zeta)^2/\{\bar{\phi}(\zeta)\cdot\bar{d}_p(\zeta)\cdot\bar{\varepsilon}(\zeta)\} \tag{3.20}$$

where $\bar{\phi}$ (ζ) is the shape factor and the drag coefficient $\bar{\Psi}$ (ζ) is defined by

$$\bar{\Psi}(\zeta)\equiv 150\{1-\bar{\varepsilon}(\zeta)\}/Re_p(\zeta)+1.75,$$

$$Re_p(\zeta)\equiv\bar{\phi}(\zeta)\cdot\bar{d}_p(\zeta)\cdot\bar{\varepsilon}(\zeta)\cdot u_g(\zeta)\rho_g/\mu_g \tag{3.21}$$

Because the value of Re_p is very large in blast furnace, the radial change in $\bar{\Psi}$ (ζ) is slight even if there existed radial changes in d_{pj} and ε_j in each layer. Hence, it may be assumed as $\bar{\Psi}(\zeta)=$const. $\equiv\Psi$. Additionally, it is assumed as $\bar{\phi}(\zeta)=\phi_1=\phi_2\equiv\phi=0.64$.

Let each volume of ore and coke burdens in a block enclosed between the radial positions ζ and $(\zeta+d\zeta)$ be designated by $V_{1\zeta}$ and $V_{2\zeta}$, respectively. Then, $\bar{\varepsilon}(\zeta)$ can be readily expressed as:

$$\bar{\varepsilon}(\zeta)=(\varepsilon_1V_{1\zeta}+\varepsilon_2V_{2\zeta})/(V_{1\zeta}+V_{2\zeta})=A+B\zeta \tag{3.22}$$

where the dimensionless factors, A and B, are related to the charging conditions through the following expressions:

$$A\equiv\{\varepsilon_1V_1+\varepsilon_2V_2+(2/3)\pi(R_1)^3\Delta(\varepsilon_1-\varepsilon_2)\}/(V_1+V_2),$$

$$B\equiv-\pi(R_1)^3\Delta(\varepsilon_1-\varepsilon_2)/(V_1+V_2),\quad \Delta\equiv\tan\alpha_2-\tan\alpha_1 \tag{3.23}$$

The mean particle size $\bar{d}_p$ (ζ) should be determined so as to meet the stipulation that the pressure drop of gas through a certain block having $\bar{\varepsilon}$ (ζ) and $\bar{d}_p$ (ζ) must be equated to the sum of that through each layer in the block. This implies that $\Delta_i/\{2\phi\bar{d}_p\bar{\varepsilon}/3(1-\bar{\varepsilon})\}$ is expressed as the sum of $\Delta_j/\{2\phi_jd_{pj}\varepsilon_j/3(1-\varepsilon_j)\}$ in each layer. Rearrangement of this expression consequently gives:

$$\bar{d}_p(\zeta)=\Delta_i\{1-\bar{\varepsilon}(\zeta)\}/\{\bar{\varepsilon}(\zeta)\cdot(C_i+D_i\zeta)\} \tag{3.24}$$

where, Δ_i, C_i and D_i are represented by:

$$\Delta_i=\Delta_{1,i}+\Delta_{2,i},\quad \Delta_{1,i}\equiv\{V_1+\pi(R_1)^3\Delta(2/3-\zeta)\}/\pi(R_i)^2,$$

$$\Delta_{2,i}\equiv\{V_2-\pi(R_1)^3\Delta(2/3-\zeta)\}/\pi(R_i)^2,$$

$$C_i\equiv\{V_1/D_{p1}+V_2/D_{p2}-(2/3)\pi(R_1)^3\Gamma\Delta/\pi(R_i)^2,\quad D_i\equiv\Gamma\Delta(R_1)^3/(R_i)^2$$

$$\Gamma\equiv 1/D_{p2}-1/D_{p1},\quad D_{pj}\equiv d_{pj}\varepsilon_j/(1-\varepsilon_j),\quad (j=1,\ 2) \tag{3.25}$$

Substituting Eq. (3.24) into (3.20), we have

$$\partial P/\partial z=\{\rho_g\Psi/(\phi\Delta_i)\}(C_i+D_i\zeta)\cdot u_g(\zeta)^2 \tag{3.26}$$

If the pressure gradient expressed by Eq. (3.26) is approximately the same at any radial position,

$$\partial(\partial P/\partial z)/\partial\zeta=0 \tag{3.27}$$

On the other hand, the mass balance regarding gas gives:

$$F_g=2\pi(R_i)^2\int_0^1\zeta\cdot\varepsilon(\zeta)\cdot u_g(\zeta)\,d\zeta \tag{3.28}$$

where F_g in Nm^3/s denotes the volume flow rate of gas at the standard state.

Combination of Eqs. (3.26) through (3.28) yields the expression for the radial velocity profile for the standard state as:

$$u_N=\frac{F_g}{2\pi(R_i)^2E_i}\frac{A+B\zeta}{\sqrt{C_i+D_i\zeta}} \tag{3.29}$$

where E_i is a dimensionless factor defined as:

$$\begin{aligned}E_i\equiv 2\{&\sqrt{C_i+D_i}[B(C_i+D_i)^2/5+(D_iA-2BC_i)\\&\times(C_i+D_i)/3-C_i(D_iA-BC_i)]-\sqrt{C_i}[B(C_i)^2/5\\&+C_i(D_iA-2BC_i)/3-C_i(D_iA-BC_i)]\}/(D_i)^3\end{aligned} \tag{3.30}$$

Equation (3.29) gives the resultant radial profile of gas flow rate, when the changes in the apparent angles of repose, ore/coke and coke base are caused by different charging arrangements.

(Ⅲ) Mathematical-kinetic Model of Blast Furnace

Because the apparent angles of repose of ore and coke differ from each other, the vertical depth of each layer varies radially. Thus, the radial distributions would be expected to concern not only the aerodynamic situation but also the thermal and the chemical aspects. Heat, mass, and momentum balances are formulated here for the region from ζ to $(\zeta+d\zeta)$ under the following assumptions:

(i) Gas and solid particles are piston flow through the specified region.

(ii) Two adjacent layers of ore and coke, as one block having the thickness Δ_i as shown in Fig. 3.1, move down instantaneously after a lapse of the residence time $\tau(=\Delta_i/u_{s,i})$ to meet the cyclic steady-state changes in process variables.

(iii) The chemical reactions to be considered here are the indirect reduction of ore and the decomposition of limestone which take place in the ore layer and the Boudouard reaction in the coke layer according to:

$$(1/3)Fe_2O_3+CO=(2/3)Fe+CO_2 \tag{3.31}$$

$$CaCO_3=CaO+CO_2 \tag{3.32}$$

$$CO_2+C=2CO \tag{3.33}$$

(1) Unsteady-state Heat Transfer in Ore and Coke Layers

By taking account of heat-in-mass transfer, the heat of reaction and the heat

exchange between gas and solid particles, the heat balance equation for the ore layer in the i-th block can be expressed as follows:

$$\frac{d(c_{s2}\rho_{b2}t_2)}{d\theta}=a_2h_{p2}(T_2-t_2)+C_{o,0}\left(\frac{df_o}{d\theta}\right)\{M_{CO}(c_p)_{CO}-M_{CO_2}(c_p)_{CO_2}\}$$
$$\times t_2-C_{l,0}\left(\frac{df_l}{d\theta}\right)M_{CO_2}(c_p)_{CO_2}t_2+C_{o,0}\left(\frac{df_o}{d\theta}\right)(-\Delta H_o)$$
$$+C_{l,0}\left(\frac{df_l}{d\theta}\right)(-\Delta H_l) \tag{3.34}$$

where t_2 and T_2 are the temperatures of solid particles and gas in the ore layer suffixed by 2, "a" denotes the specific surface area, ρ_b is the bulk density, $C_{o,0}$ and $C_{l,0}$ refer to the initial molar concentrations of combined oxygen and $CaCO_3$, respectively, f's are the fractional conversions, c's are the specific heats, M's stand for the molecular masses, $(-\Delta H)$'s denote the heats of reaction, and θ is the time.

The change in the bulk density of the ore layer caused by the progress of the reactions can be expressed by:

$$\rho_{b2}=\rho_{b2,0}-(16C_{o,0}f_o+44C_{l,0}f_l) \tag{3.35}$$

Substituting Eq. (3.35) into Eq. (3.34), and assuming that the gas temperature in the ore layer may be kept at $T_{2,i}$ during the period τ, the resultant heat transfer equation can be obtained as:

$$dt_2/d\theta=K_2(T_{2,i}-t_2)+H_o(-\Delta H_o)+H_l(-\Delta H_l)+\{H_o[28(c_p)_{CO}$$
$$-44(c_p)_{CO_2}+16c_{s2}]+44H_l[c_{s2}-(c_p)_{CO_2}]\}\cdot t_2 \tag{3.36}$$

where K_2 and $H_k(k=o,\ l)$ are defined as follows:

$$K_2\equiv a_2h_{p2,i}/\rho_{b2}\{c_{s2}+t_2(dc_{s2}/dt_2)\},$$
$$H_k\equiv C_{k,0}(df_k/d\theta)/\rho_{b2}\{c_{s2}+t_2(dc_{s2}/dt_2)\},\quad (k=o,\ l) \tag{3.37}$$

In an analogous manner, heat balance equation for the coke layer and its bulk density can be represented by Eqs. (3.38) and (3.40), respectively.

$$dt_1/d\theta=K_1(T_{1,i}-t_1)+H_c(-\Delta H_c)+H_c[44(c_p)_{CO_2}-56(c_p)_{CO}+12c_{s1}]t_1 \tag{3.38}$$

where t_1 is the temperature of solid particles in the coke layer suffixed by 1, $-\Delta H_c$ denotes the heat of Boudouard reaction, and K_1 and H_c are defined as follows:

$$K_1\equiv a_1h_{p1,i}/\rho_{b1}\{c_{s1}+t_1(dc_{s1}/dt_1)\},$$
$$H_c\equiv C_{c,0}(df_c/d\theta)/\rho_{b1}\{c_{s1}+t_1(dc_{s1}/dt_1)\} \tag{3.39}$$
$$\rho_{b1}=\rho_{b1,0}-12C_{c,0}f_c \tag{3.40}$$

where f_c denotes the fractional gasification of carbon.

(2) Overall Heat Balance in Ore and Coke Layers

Integration of Eq. (3.34) from 0 to τ with respect to θ will give the heat balance equation in the ore layer in the form of Eq. (3.44) described later. In carrying out the intergration, the relations which will follow have been taken into account.

Taking the overall heat belance for gas side, we have:

$$(A_i\Delta_{2,i})a_2h_{p2}\int_0^\tau(T_2-t_2)d\theta+\int_0^\tau\{C_{o,0}(df_o/d\theta)\times[M_{CO}(c_p)_{CO}-M_{CO_2}(c_p)_{CO_2}]t_2-C_{l,0}(df_l/d\theta)M_{CO_2}(c_p)_{CO_2}t_2\}d\theta=\int_0^\tau\{(G_gc_gT_2)_{in}-(G_gc_gT_2)_{out}\}d\theta-2\pi\zeta R_i\Delta_{2,i}(\hat{\xi}U)\int_0^\tau(t_2-T_{cw})d\theta \quad (3.41)$$

where A_i is the cross-sectional area of the i-th blok of burdens, U denotes the overall heat transfer coefficient and T_{cw} is the temperature of the cooling water around the furnace. The first and the second terms of integrals in the left-hand side of Eq. (3.41) represent the amounts of heat transferred by the heat exchange between gas and solid particles and by the heat-in-mass transfer, respectively. Each integral term on the right-hand side shows the change in the heat content of the gas and the heat transferred in the radial direction, respectively.

To estimate the value of the correction factor ξ, an effective thermal conductivity[4] has been applied for analyzing the observed temperature distribution in a cylindrical bed[5]. As a result, the following simple correlation has been obtained. That is, $\xi=\zeta$.

For the sake of further simplification, the terms involved in each integral in the right-hand side of Eq. (3.41) and the heats of reaction, $(-\Delta H_k)$ $(k=o,l)$ are assumed to be kept constant throughout the period τ. Namely,

$$-\Delta H_k=-\Delta H_{k,i},\quad (k=o,\ l),$$
$$(G_gc_gT_2)_{in}-(G_gc_gT_2)_{out}=(F_g\rho_gc_gT)_{1,i}-(F_g\rho_gc_gT)_{2,i},$$
$$T_2=T_{2,i} \quad (3.42)$$

Equation (3.41) subject to Eq. (3.42) ultimately yields the expression for the temperature of gas entering into the ore layer of the i-th block as follows:

$$T_{1,i}=L_{2,i}T_{2,i}+\gamma_{2,i}(\Delta_{2,i}/\Delta_i)(t_{2,i}-M_{2,i}t_{2,i-1}-\Delta T_{o,i}-\Delta T_{l,i})+N_{2,i}(T_{2,i}-T_{cw}) \quad (3.43)$$

where

$$\gamma_{2,i}\equiv F_s(\rho_bc_s)_{2,i}/(F_g\rho_gc_g)_{1,i},\quad L_{2,i}\equiv(F_g\rho_gc_g)_{2,i}/(F_g\rho_gc_g)_{1,i},$$
$$M_{2,i}\equiv(\rho_bc_s)_{2,i-1}/(\rho_bc_s)_{2,i},\quad N_{2,i}\equiv2\pi\zeta R_i\Delta_{2,i}\hat{\xi}U/(F_g\rho_gc_g)_{1,i},$$
$$\Delta T_{k,i}\equiv C_{k,0}(f_{k,i}-f_{k,i-1})(-\Delta H_{k,i})/(\rho_bc_s)_{2,i},\quad (k=o,\ l) \quad (3.44)$$

where F_s denotes the volume flow rate of solid particles.

In Eqs. (3.43) and (3.44), variables, t_2, f_k, ρ_{b2} and c_{s2}, with suffix i are defined as the values at $\theta=\tau$.

The temperature of gas entering into the coke layer can be likewise written as follows:

$$T_{2,i+1}=L_{1,i}T_{1,i}+\gamma_{1,i}(\Delta_{1,i}/\Delta_i)(t_{1,i}-M_{1,i}t_{1,i-1}-\Delta T_{c,i}) \\ +N_{1,i}(T_{1,i}-T_{cw}) \tag{3.45}$$

where

$$\gamma_{1,i}\equiv F_s(\rho_b c_s)_{1,i}/(F_g\rho_g c_g)_{2,i+1},\quad L_{1,i}\equiv(F_g\rho_g c_g)_{1,i}/(F_g\rho_g c_g)_{2,i+1}, \\ M_{1,i}\equiv(\rho_b c_s)_{1,i-1}/(\rho_b c_s)_{1,i},\quad N_{1,i}\equiv 2\pi\zeta R_i\Delta_{1,i}\bar{\alpha}U/(F_g\rho_g c_g)_{2,i+1}, \\ \Delta T_{c,i}\equiv C_{c,0}(f_{c,i}-f_{c,i-1})(-\Delta H_{c,i})/(\rho_b c_s)_{1,i} \tag{3.46}$$

In Eqs. (3.45) and (3.46), variables, t_1, f_c ,ρ_{b1}, and c_{s1}, with suffix i are defined as the respective values at $\theta=\tau$.

It should be noted in Eqs. (3.43) and (3.45) that the gas temperature in layered burdens case is governed by three thermal flow ratios (γ, L, and M) instead of γ alone for a homogeneously mixed burden.

(3) Overall Mass Balances in Ore and Coke Layers

Taking the mass balance with respect to total gas during the period τ, the average flow rates of gas entering into ore and coke layers of the i-th block can be represented algebraically by Eqs. (3.47) and (3.48), respectively.

$$F_{g1,i}=F_{g2,i}(1-\Delta Y_{l,i}) \tag{3.47}$$

$$F_{g2,i}=F_{g1,i}(1-\Delta Y_{c,i}) \tag{3.48}$$

where $\Delta Y_{l,i}$ and $\Delta Y_{c,i}$ denoting the dimensionless volume changes of carbon dioxide are defined according to:

$$\Delta Y_{k,i}\equiv 22.4C_{k,0}(f_{k,i}-f_{k,i-1})(F_s/F_{g2,i})(\Delta_{2,i}/\Delta_i),\quad (k=o,\ l) \\ \Delta Y_{c,i}\equiv 22.4C_{c,0}(f_{c,i}-f_{c,i-1})(F_s/F_{g1,i})(\Delta_{1,i}/\Delta_i) \tag{3.49}$$

The molar fractions of gas species entering into the ore and coke layers can be obtained from mass balances.

Namely, from CO balance for each layer we have:

$$y_{CO,1,i}=(y_{CO,2,i}+\Delta Y_{o,i})/(1-\Delta Y_{l,i}) \tag{3.50}$$

$$y_{CO,2,i+1}=(y_{CO,1,i}-2\Delta Y_{c,i})/(1-\Delta Y_{c,i}) \tag{3.51}$$

Similarly, from CO_2 balances, we have:

$$y_{CO_2,1,i}=(y_{CO_2,2,i}-\Delta Y_{o,i}-\Delta Y_{l,i})/(1-\Delta Y_{l,i}) \tag{3.52}$$

$$y_{CO_2,2,i}=(y_{CO_2,1,i}+\Delta Y_{c,i})/(1-\Delta Y_{c,i}) \tag{3.53}$$

Also, from H_2, H_2O and N_2 balances, we have

$$h_{1,i}=h_{2,i}(1-\Delta Y_{l,i}) \quad (h=y_{H_2},\ y_{H_2O},\ y_{N_2}) \tag{3.54}$$

$$h_{2,i+1}=h_{1,i}(1-\Delta Y_{c,i}) \quad (h=y_{H_2},\ y_{H_2O},\ y_{N_2}) \tag{3.55}$$

Summing up the products of density of each component of gas and its composition represented by Eqs. (3.50) to (3.55), the average densities of gas entering into each layer can be expressed as follows:

$$\rho_{g1,i}=(\rho_{g2,i}-0.727\Delta Y_{o,i}-1.977\Delta Y_{l,i})/(1-\Delta Y_{l,i}) \tag{3.56}$$

$$\rho_{g2,i+1}=(\rho_{g1,i}-0.523\Delta Y_{c,i})/(1-\Delta Y_{c,i}) \tag{3.57}$$

(4) Pressure Drop of Gas Flowing through Ore and Coke Layers

Pressure drop of gas passing through each layer of burdens with thickness of $\Delta_{j,i}$ can be evaluated on the basis of the Ergun formula described by Eq. (3.20), Then, the gas pressure at the lowest end of each layer is given as follows:

$$P_{1,i}=P_{2,i}+\Delta P_{2,i} \tag{3.58}$$

$$P_{2,i+1}=P_{1,i}+\Delta P_{1,i} \tag{3.59}$$

(5) Numerical Method for Computation

The mathematical kinetic model mentioned above, combined with the radial profile of the gas velocity given by Eq. (3.29), allows us to predict the longitudinal variations of the process variables along each dimensionless radius of the lumpy zone provided the initial conditions have been specified at the top of the bed. Figure 3.2 schematically illustrates the interrelation among the temperatures shown in Fig. 3.1. A combination of the temperatures, $t_{2,i-1}$ and $T_{2,i}$ according to the unsteady-state heat transfer equation gives the temperature $t_{2,i}$. A subsequent combination of the temperatures, $t_{2,i-1}$, $T_{2,i}$ and $t_{2,i}$, according to the overall heat balance equation leads to the temperature $T_{1,i}$. The obtained $T_{1,i}$ follows to combine with $t_{1,i-1}$ according to the unsteady-state heat transfer equation to yield the temperature $t_{1,i}$. Such calculating procedure, which may be successively continued till the melting point of ore, consequently results in the radial as well as the longitudinal distributions of the process variables in the layered lumpy zone of blast furnace. Detailed discussion with respect to computed results is available elsewhere[2,3].

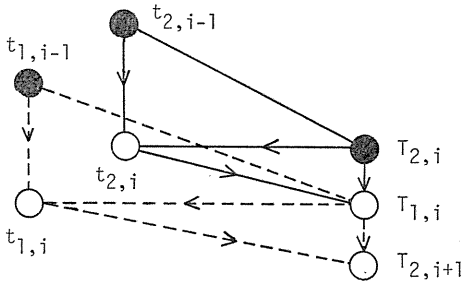

Fig. 3. 2. Procedure for temperature calculation.

3. 3. Sintering Machine

(1) Introduction

The commonly used Dwight-Lloyd sintering machine involves a moving bed of granulated solid materials which are crossly countered by the down draught air to propagate the reaction zone, gradually raising the temperature of solid particles to the level at which fusion of particles can occur.

This DL sintering system has been mathematically formulated[6~12] on the basis

of the balances for the heat and mass transfer processes. In this section, the governing equations for preheating, cooling and combustion zones of the DL sintering bed are derived from a set of generalized equations which allows to cover various problems on the moving bed as well as the fixed bed systems. Notation employed is basically the same as in section 2.

(2) Mathematical Formulation

(i) Overall Continuity

For a gas-solid reactor involving the convective flow as well as the mass generation by chemical reactions, the overall mass conservation per unit volume of bed is expressed in general form as:

$$\varepsilon_j(\partial\rho_j/\partial\theta) = -\mathrm{div}\vec{G}_j + \delta_j\textstyle\sum_i\beta_i R_i^*, \quad (j=g,\ s) \tag{3.60}$$

where $\delta_g=1$ and $\delta_s=-1$, ε_j is the fractional volume ($\varepsilon_g=\varepsilon$, $\varepsilon_s=1-\varepsilon$), ρ_j is the density ($\rho_g=\rho_g$, $\rho_s=\rho_p$), θ is the time, and R_i^* denotes the overall reaction rate. β_i is the rate of mass generation defined by $\sum_k(\nu_{ki}M_k)_g$ where ν_{ki} is the stoichiometric coefficient for species k appearing in the i-th reaction and $\nu_{ki}>0$ for generation of species k whereas $\nu_{ki}<0$ for its dissipation, and M_k denotes the molecular mass, $\vec{G}_j$ is the mass velocity vector expressed by:

$$\vec{G}_j = \rho_j\varepsilon_j\vec{u}_j \tag{3.61}$$

where u_j designates the moving speed of solid or the linear velocity of gas.

For the DL sintering process, we now proceed to derive the overall continuity equation from Eq. (3.60). In developing the mathematical formulation, this process is usually handled as two-dimensional system with the coordinates of x and z which denote the moving direction of the pallet and the downward direction, respectively.

Assuming that the gas is flowing only downwards (thus $G_{gx}=0$) and the accumulation term for gas phase is negligible, we can readily reduce Eq. (3.60) for the gas phase to the following:

$$\partial G_{gz}/\partial z = \textstyle\sum_i\beta_i R_i^* \tag{3.62}$$

For the solid phase with no downward movement and with a constant pallet speed, u_{sx}, Eq. (3.60) consequently leads to:

$$(1-\varepsilon)(\partial\rho_s/\partial\theta) = -u_{sx}[\partial\{\rho_s(1-\varepsilon)\}/\partial x] - \textstyle\sum_i\beta_i R_i^* \tag{3.63}$$

Assuming the bed voidage to be kept constant during sintering, we can rewrite Eq. (3.63) into:

$$D\rho_b/D\theta = -\textstyle\sum_i\beta_i R_i^* \tag{3.64}$$

where $\rho_b=\rho_s\ (1-\varepsilon)$ is the bulk density and the substantial derivative is defind as $D\rho_b/D\theta=\partial\rho_b/\partial\theta+u_{sx}(\partial\rho_b/\partial x)$, represening a derivative on the coordinate moving with pallet.

(ii) Continuity of Species

For a species k in the j-th multicomponent phase, the conservation principle can be given by:

$$\varepsilon_j(\partial C_{jk}/\partial\theta) = -\mathrm{div}\vec{N}_{jv} - \mathrm{div}\vec{N}_{jd} + \textstyle\sum_i\nu_{ki}R_i^*, \quad (j=g,\ s) \tag{3.65}$$

where C_{jk} denotes the molar concentration, the third term on the right-hand side expresses the generation rate of k-th species per unit volume of bed, and $-\mathrm{div}\vec{N}_{jv}$ and $-\mathrm{div}\vec{N}_{jd}$ stand for the net rates of inflow by the convection and the diffusion, respectively. The convective molar flux $\vec{N}_{jv}$ and the diffusive molar flux $\vec{N}_{jd}$ can be represented by:

$$\vec{N}_{jv}=C_{jk}\varepsilon_j\vec{u}_j \tag{3.66}$$

$$\vec{N}_{jd}=(-D_{jx}(\partial C_{jk}/\partial x),\quad -D_{jz}(\partial C_{jk}/\partial z)) \tag{3.67}$$

where D_{jn} denotes the dispersion coefficient.

For the DL sintering process, we can eliminate the dispersion term entirely. Hence, Eq. (3.65) subject to the assumptions that $u_{gx}=0$, $u_{sx}=$constant and $u_{sz}=0$, consequently results in the following expressions for gas and the solid phases.

$$\varepsilon(\partial C_{gk}/\partial\theta)=-\partial(C_{gk}\varepsilon u_{gz})/\partial z+\textstyle\sum_i\nu_{ki}R_i^* \tag{3.68}$$

$$(1-\varepsilon)[\partial C_{sk}/\partial\theta]=-u_{sx}[\partial\{C_{sk}(1-\varepsilon)\}/\partial x\}+\textstyle\sum_i\nu_{ki}R_i^* \tag{3.69}$$

Equation (3.69) is rewritten as:

$$D\{C_{sk}(1-\varepsilon)\}/D\theta=\textstyle\sum_i\nu_{ki}R_i^* \tag{3.70}$$

where $C_{sk}(1-\varepsilon)$ represents the molar concentration per unit volume of bed.

(iii) Heat Balance

Taking the terms related to mass flow, conduction, heat exchange and heat generation by chemical reaction into consideration, we can express the conservation equation of thermal energy in the form:

$$\varepsilon_j\{\partial(c_j\rho_jT_j)/\partial\theta\}=-\mathrm{div}\vec{q}_{jv}-\mathrm{div}\vec{q}_{jd}-\delta_jh_pa(T_g-T_s)+\eta_j\textstyle\sum_iR_i^*(-\Delta H_i),$$

$$(j=g,\ s) \tag{3.71}$$

where $\delta_g=1$, $\delta_s=-1$, $\eta_g+\eta_s=1$, c_j is the specific heat, T_j is the temperature, h_p is the heat transfer coefficient between gas and solid particle, a is the specific surface area, ΔH stands for the enthalpy change accmpanied by chemical reactions or phase transformations, η_j is the fractional heat acquisition of heat of reactions including the extent of heat-in-mass transfer, and the convective heat flux $\vec{q}_{jv}$ and the conductive heat flux $\vec{q}_{jd}$ can be represented as follow:

$$\vec{q}_{jv}=c_jT_j\vec{G}_j \tag{3.72}$$

$$\vec{q}_{jd}=(-K_{jx}(\partial T_j/\partial x),\ -K_{jz}(\partial T_j/\partial z)) \tag{3.73}$$

In the case of DL sintering process, owing to the lack of information concerning the value of η_j, we often assume as $\eta_g=0$. As for the heat balance equation for the gas phase, this assumption together with the additional assumptions neglecting both the heat accumulation and the heat conduction terms, consequently transforms Eq. (3.71) into:

$$\mathrm{div}(c_g T_g \vec{G}_g) + h_p a (T_g - T_s) = 0 \tag{3.74}$$

Equation (3.74) is rewritten into:

$$\vec{G}_g \cdot \mathrm{grad}(c_g T_g) = -c_g T_g \mathrm{div}\vec{G}_g - h_p a (T_g - T_s) \tag{3.75}$$

Based on the assumption that $G_{gx}=0$, Eq. (3.75) reduces to:

$$G_{gz}\{\partial(c_g T_g)/\partial z\} = -c_g T_g (\partial G_{gz}/\partial z) - h_p a (T_g - T_s) \tag{3.76}$$

Substituting Eq. (3.62) into Eq. (3.76), we ultimately obtain the expression as:

$$G_{gz}\{\partial(c_g T_g)/\partial z\} = -c_g T_g \textstyle\sum_i \beta_i R_i^* - h_p a (T_g - T_s) \tag{3.77}$$

As for the heat balance equation for the solid phase, Eq. (3.71) leads to:

$$\varepsilon_s\{\partial(c_s \rho_s T_s)/\partial\theta\} = -\mathrm{div}(c_s T_s \vec{G}_s) + h_p a (T_g - T_s) + \textstyle\sum_i R_i^* (-\Delta H_i) \tag{3.78}$$

In Eq. (3.78) assuming that $u_{sx}=$constant, $u_{sz}=0$, and $\varepsilon=$constant, we have

$$c_s T_s (D\rho_b/D\theta) + \rho_b \{D(c_s T_s)/D\theta\} = h_p a (T_g - T_s) + \textstyle\sum_i R_i^* (-\Delta H_i) \tag{3.79}$$

Substituting Eq. (3.64) into Eq. (3.79), we obtain

$$\rho_b \{D(c_s T_s)/D\theta\} = c_s T_s \textstyle\sum_i \beta_i R_i^* + h_p a (T_g - T_s) + \sum_i R_i^* (-\Delta H_i) \tag{3.80}$$

(iv) Momentum Transfer

The vectorial Ergun equation for gas is expressed as:

$$\mathrm{grad}\, P = -(f_1 + f_2 |\vec{G}_g|)\vec{G}_g \tag{3.81}$$

For the sintering process with $G_{gx}=0$, Eq. (3.81) is reduced to:

$$\partial P/\partial z = -(f_1 + f_2 |G_{gz}|) G_{gz} \tag{3.82}$$

which allows to evaluate the mass velocity of gas under the given back pressure.

(v) Auxiliary Relations

For the i-th reaction considered, the stoichiometric coefficient ν_{ki} and β_i associated with the mass generation are, for example, as follows:

$$\text{(reaction 1)} \quad \mathrm{C} + \mathrm{O_2} \rightarrow \mathrm{CO_2} : \nu_{\mathrm{O_2},1} = -1,\ \nu_{\mathrm{CO_2},1} = 1,\ \beta_1 = M_{\mathrm{CO_2}} - M_{\mathrm{O_2}} = M_{\mathrm{C}} \tag{3.83}$$

$$\text{(reaction 2)} \quad \mathrm{CaCO_3} \rightarrow \mathrm{CaO} + \mathrm{CO_2} : \nu_{\mathrm{O_2},2} = 0,\ \nu_{\mathrm{CO_2},2} = 1,\ \beta_2 = M_{\mathrm{CO_2}} \tag{3.84}$$

In order that the DL sintering machine can be fully described, we would require to formulate some other phenomena including drying of solid particles,

melting and solidification, mineralogical changes, etc. that occur during the sintering process. Preliminary approaches to these problems may be available in the literatures[6~12]. In recent years, detailed investigations have been devoted to the clarification of the change in permeability of bed during sintering process. Shibata et al.[13,14] measured the permeability in each characteristic zone in a sintering pot. Kasai et al.[15] formulated the transitional changes in voidage and apparent size of solid particles on the basis of the information obtained from a laboratory-scale sintering simulator. Sato et al.[16] proposed a comprehensive model to interrelate the melting process in sintering to the physical and chemical properties of iron ore.

3. 4. Moving Bed Reactor

(1) Introduction

The moving bed reactor is advantageous for the continuous processing of solid particles. Current topics on the transport phenomena in this reactor are reviewed elsewhere[17]. In this section, the generalized formulation and the thermal characteristics of the moving bed reactor are outlined.

(2) Generalized Formulation for Distributed System

As described in the preceding section, the vectorial conservation equations characterizing also the moving bed reactor take the forms as Eq. (3. 60) for total mass, Eq. (3. 65) for each chemical species, Eq. (3. 71) for heat, and Eq. (3. 81) for momentum transfer.

A combination of these equations with the appropriate intial and boundary conditions completes the statement of this system and may be numerically solved in the finite-difference forms.

(3) One-dimensional Heat Transfer Process

From the generalized conservation equations mentioned above, we now derive the fundmental equations describing the one-dimensional heat transfer process in the co- and the counter-current moving beds. Assumptions made in developing the present formulation are as follows:

(i) The system is assumed to be in steady state.
(ii) Gas and solid materials are assumed to flow straight, without thermal conduction
(iii) The wall is assumed to be impervious to heat flow.
(iv) Thermal properties are assumed to be kept constant.

The assumptions (i) and (ii) allow to write as $\partial(c_j\rho_j T_j)/\partial\theta=0$ and $\vec{q}_{jd}=0$ in Eq. (3. 71) representing the heat transfer process, thus we have the following expression for $j(=g,s)$ phase:

$$-\mathrm{div}(c_j T_j \vec{G}_j)-\delta_j h_p a(T_g-T_s)+\eta_j\textstyle\sum_i R_i^*(-\Delta H_i)=0 \qquad (3.85)$$

Equation (3. 85) can be rewritten as:

$$c_j T_j \,\mathrm{div}\,\vec{G}_j+\mathrm{grad}(c_j T_j)\cdot\vec{G}_j+\delta_j h_p a(T_g-T_s)-\eta_j\textstyle\sum_i R_i^*(-\Delta H_i)=0 \qquad (3.86)$$

Combining the relation $\mathrm{div}\vec{G}_j=\delta_j\sum_i\beta_i R_i^*$, which can be derived from the overall continuity equation written by Eq. (3. 60), with constant specific heat c_j, conse-

quently Eq. (3.86) can be expressed as

$$c_j\vec{G}_j\cdot\mathrm{grad}\,T_j+\delta_j h_p a(T_g-T_s)+\delta_j c_j T_j\sum_i\beta_i R_i^*-\eta_j\sum_i R_i^*(-\Delta H_i)=0 \tag{3.87}$$

Equation (3.87) in the one-dimensional system with z-direction takes the form:

$$\text{(gas side)} \quad : \quad c_g G_{gz}(dT_g/dz)+h_p a(T_g-T_s)+c_g T_g\sum_i\beta_i R_i^* -\eta_g\sum_i R_i^*(-\Delta H_i)=0 \tag{3.88}$$

$$\text{(solid side)} \quad : \quad c_s G_{sz}(dT_s/dz)-h_p a(T_g-T_s)-c_s T_s\sum_i\beta_i R_i^* -\eta_s\sum_i R_i^*(-\Delta H_i)=0 \tag{3.89}$$

It should be noted here that the component of the mass-velocity vector, in the z-direction, $G_{jz}(j=g,\ s)$, is positive when the j-phase is moving in the positive direction of z, and vice versa.

These two equations are rewritten in dimensionless forms as:

$$dT_g^*/dz^*=-St(T_g^*-T_s^*)-S_1T_g^*+\eta_g S_2 \tag{3.90}$$

$$dT_s^*/dz^*=-(St/\gamma)(T_g^*-T_s^*)+(S_1/S_3)T_s^*-\eta_s S_2/\gamma \tag{3.91}$$

with the dimensionless parameters defined by:

$$\begin{aligned} &T_g^*\equiv T_g/T_{g0},\quad T_s^*\equiv T_s/T_{g0},\quad z^*\equiv z/L,\\ &St\equiv h_p aL/c_g G_{gz},\quad \gamma\equiv -c_s G_{sz}/c_g G_{gz},\\ &S_1\equiv L\sum_i\beta_i R_i^*/G_{gz},\quad S_2\equiv L\sum_i R_i^*(-\Delta H_i)/c_g G_{gz}T_{g0},\\ &S_3\equiv G_{sz}/G_{gz} \end{aligned} \tag{3.92}$$

where St stands for the Stanton number and γ refers to the thermal flow ratio. Here, γ is positive for the counter-current bed as seen in the case of blast furnace, and negative for the co-current bed because of the sign of G_{jz}.

The boundary conditions for gas and solid particles are specified at the two ends of the reactor in the case of the counter-current moving bed, whereas at the same inlet position in the co-current case. In the absence of chemical reactions, the exponential type solution to this problem has been well known hitherto[18,19].

Now we proceed to correlate the gas-to-solid heat exchanging regime without chemical reactions explicitly to the value of the thermal flow ratio for the case of counter-current moving bed. The effect of chemical reactions is neglected here, thus $S_1=S_2=0$.

(i) Interrelation between dT_g^*/dz^* and dT_s^*/dz^*

Combination of Eqs. (3.90) and (3.91) results in:

$$dT_g^*/dz^*=\gamma(dT_s^*/dz^*) \tag{3.93}$$

(ii) Axial variation of $(T_g^*-T_s^*)$

Subtraction of Eq. (3.91) from Eq. (3.90) consequently gives:

$$I_1 \equiv d(T_g^* - T_s^*)/dz^* = \{(St)/\gamma\}(1-\gamma)(T_g^* - T_s^*) \tag{3.94}$$

Taking the relation $(T_g^* - T_s^*) > 0$ into consideration, we have

$$I_1 > 0 \text{ for } \gamma < 1, \quad I_1 = 0 \text{ for } \gamma = 1, \quad I_1 < 0 \text{ for } \gamma > 1 \tag{3.95}$$

(iii) Curvature of temperature profile

Differentiation of Eq. (3.90) with respect to z^*, together with Eqs. (3.90) and (3.91), leads to the following relations:

$$I_2 = d^2T_g^*/dz^{*2} = \gamma(d^2T_s^*/dz^{*2}) = (St)^2(T_g^* - T_s^*)(\gamma - 1)/\gamma \tag{3.96}$$

$$I_2 < 0 \text{ for } \gamma < 1, \quad I_2 = 0 \text{ for } \gamma = 1, \quad I_2 > 0 \text{ for } \gamma > 1 \tag{3.97}$$

On the basis of the relations from Eqs. (3.93) to (3.97), we can elucidate the general characteristics of the temperature profile in the counter-current moving bed heat exchanger.

Furthermore, the temperature profile in the upper part of blast furnace, where the heat of reaction is negligible, may correspond to the situation for the case of $\gamma < 1$.

Nomenclature

A : cross-sectional area of the top of furnace (m^2)
a : specific surface area (m^2/m^3(bed))
C : specific heat of gas (J/kg·K)
C_{jk} : molar concentration of k-th component in j-phase (kmol/m^3)
$C_{c,0}$: initial concentration of carbon in coke layer (kmol/m^3(coke bed))
$C_{l,0}$: initial concentration of $CaCO_3$ in ore layer (kmol/m^3(ore bed))
$C_{o,0}$: initial concentration of oxygen combined with iron in ore layer (kmol/m^3(ore bed))
c : specific heat of solid particle (J/kg·K)
c_j : specific heat of j-phase (J/kg·K)
D : dispersion coefficient (m^2/s)
d_p : diameter of solid particle (m)
$\bar{d}_p$: particle size longitudinally averaged over adjacent two layers (m)
F_b : blast volume (Nm^3/s)
F_g : volume flow rate of gas (Nm^3/s)
F_s : volume flow rate of solid particles (m^3(bed)/s)
f : fractional conversion (−)
G_j : mass velocity of j-phase (kg/m^2·s)
$-\Delta H_i$: heat of reaction (J/kmol)
h_p : heat transfer coefficient between gas and solid particle (W/m^2·K)
K_j : effective thermal conductivity (W/m·K)
L : bed height (m)
M_k : molecular mass of component k (kg/kmol)
$\vec{N}_j$: molar flux vector (kmol/m^2·s)
$(\%N_2)$: mean concentration of N_2 in exhaust gas (%)

n : number of charges per hour (1/3600s)
P : gas pressure (Pa)
$\vec{q}$: heat flux vector (W/m²)
R_i : mean radius of i-th block in blast furnace (m)
R^* : overall reaction rate (kmol/m³(bed)·s)
Re_p : particle Reynolds number (−)
r : radial distance (m)
St : Stanton number (−)
T : gas temperature (K)
T_j : temperature of j-phase (K)
$T_{j,i}$: temperature of gas through j-th layer in i-th block of burden (K)
T_m : mean temperature of top gas changing transitionally from T_0 to T_z (K)
T_0 : temperature of top gas at the time immediately after the charging is finished (K)
T_z : temperature of top gas at the time just before the next charge is fed (K)
t : temperature of solid particle (K)
U : overall heat transfer coefficient (W/m²·K)
u_j : linear velocity of j-phase (m/s)
u_N : superficial flow rate of gas (Nm³/m²(bed)·s)
u_s : descending velocity of solid particles (m/s)
V_j : volume of j-th layer per one charge (m³(bed))
W : mass flow rate of gas (kg/s)
w : mass flow rate of solid particles (kg/s)
w_c, w_o : mass of coke and iron ore per one charge, respectively (kg)
x : distance (m)
y_k : molar fraction of component k (−)
z : distance (m)
α_j : apparent angle of repose of j−th layer (j=1,2) (−)
β : rate of mass generation (kg/kmol)
γ : thermal flow ratio (−)
Δ_i : vertical depth of i-th block (m)
$\Delta_{j,i}$: vertical depth of j-th layer in i-th block (m)
$\varepsilon_j(j=1, 2)$: voidage of j-th layer (−)
$\varepsilon_j(j=g, s)$: fractional volume of j-phase (m³/m³(bed))
$\bar{\varepsilon}$: mean voidage of adjacent two layers (−)
ζ : dimensionless radius ($=r/R_i$) (−)
η : fractional acquisition of heat of reaction (−)
θ : time (s)
μ : viscosity (Pa·s)
ν_{ki} : stoichiometric coefficient for species k appearing in i-th reaction (−)
ξ : correction factor of U (−)
ρ : density of gas (kg/Nm³)
ρ_b : bulk density (kg/m³)
ρ_c, ρ_o : bulk density of coke layer and iron ore layer, respectively (kg/m³(bed))
$\rho_{j(j=g,s)}$: density of j-phase (kg/m³)
τ : residence time of solid particles in each block (s)
ϕ : shape factor (−)
$\bar{\phi}$: mean ϕ of adjacent two layers (−)
Ψ : drag coefficient of Ergun equation (−)

$\overline{\Psi}$: mean Ψ of adjacent two layers (−)

(Subscripts)

0 : inlet conditions, c : coke, cw : cooling water, d : conduction,

i : block number marked from top level to tuyere level of blast furnace, or kind of reaction, in : inflow, j : layer number (1 : coke, 2 : ore), or phase number (g : gas, s : solid), k : chemical species, l : limestone, o : ore,

out : outflow, p : particle, v : convection, x : lateral direction, z : axial direction

References

1) Tamura, K., "Seiren Kagaku Kōgaku Enshu", ed. by Muchi, I., 75, Yokendo, (1974).
2) Kuwabara, M. and Muchi, I., Trans. ISIJ, 17, 271 (1977).
3) Kuwabara, M. and Muchi, I., Trans. ISIJ, 17, 321 (1977).
4) Coberley, C. A. and Marshall, W. R., Chem. Eng. Progr., 47, 141 (1951).
5) Smith, J. M., "Chemical Engineering Kinetics", 294, McGraw-Hill, (1956).
6) Higuchi, J. and Muchi, I., Tetsu-to-Hagané, 53, 1171 (1967).
7) Muchi, I. and Higuchi, J., Tetsu-to-Hagané, 56, 371 (1970).
8) Muchi, I. and Higuchi, J., Trans. ISIJ, 12, 54 (1972).
9) Tukamoto, T., Simada, S., Taguchi, T. and Higuchi, J., Tetsu-to-Hagané, 56, 661 (1970).
10) Hamada, T., Koitabashi, T. and Okabe, K., Tetsu-to-Hagané, 53, 1567 (1972).
11) Horio, M., Ohtake, T. and Muchi, I., Tetsu-to-Hagané, 60, 465 (1972).
12) Young, R. W., Ironmaking & Steelmaking, 4, 321 (1977).
13) Wajima, M., Hosotani, Y., Shibata, J., Soma, H. and Tashiro, K., Tetsu-to-Hagané, 68, 1719 (1982).
14) Shibata, J., Wajima, M., Soma, H. and Matsuoka, H., Tetsu-to-Hagané, 70, 178 (1984).
15) Kasai, E., Yagi, J. and Omori, Y., Tetsu-to-Hagané, 70, 1567 (1984).
16) Sato, S., Kawaguchi, T., Ichidate, M. and Yoshinaga, M., Tetsu-to-Hagané, 70, 657 (1984).
17) Kuwabara, M. and Muchi, I., Kagaku Kōgaku, 47, 688 (1983).
18) Furnace, C. C., Ind. Eng. Chem., 22, 26 (1930).
19) Elliot, J. F., Trans. Met. Soc. AIME, 227, 802 (1963).

Part 2 Modelling of steelmaking processes

4. Fundamental principles in theoretical analysis

4. 1. Application of Navier-Stokes Equation

(1) Introduction

In many practical operations of metallurgical processes fluid motion plays an important role together with mass and heat transfer phenomena. The fluid motion observed in these operations is turbulent, in which irregular fluctuations, eddying motions and random mixing are superimposed on the stream.

The quantitative description of the fluid flow phenomena would be helpful for

a better understanding of metallurgical processes. In the following we shall present a general mathematical statement of the fluid flow including recirculating turbulent flow.

(2) Formulation

Let us consider the steady flow of the incompressible Newtonian fluid in an axi-symmetric cylindrical or a two-dimentional cartesian coordinate system. Now we designate the distances along the axial or longitudinal coordinate and the radial or lateral coordinate by Z_1 and Z_2, respectively, and also we refer to V_1 and V_2 as the corresponding components of velocity.

The equation of continuity is given by the expression

$$\frac{\partial(\rho V_1)}{\partial Z_1}+\frac{1}{\xi}\frac{\partial(\rho\xi V_2)}{\partial Z_2}=0 \tag{4.1}$$

where $\xi=Z_2$ is adopted in cylindrical coordinates and $\xi=1$ in cartesian coordinates.

The equation of motion is expressed by Eq. (4.2) in the axial or longitudinal coordinate and by Eq. (4.3) in the radial or lateral coordinate.

$$\rho\left(V_1\frac{\partial V_1}{\partial Z_1}+V_2\frac{\partial V_1}{\partial Z_2}\right)=-\frac{\partial P}{\partial Z_1}+\mu\left[\frac{1}{\xi}\frac{\partial}{\partial Z_2}\left(\xi\frac{\partial V_1}{\partial Z_2}\right)+\frac{\partial^2 V_1}{\partial Z_1^2}\right]+f_1 \tag{4.2}$$

$$\rho\left(V_2\frac{\partial V_2}{\partial Z_2}+V_1\frac{\partial V_2}{\partial Z_1}\right)=-\frac{\partial P}{\partial Z_2}+\mu\left[\frac{\partial}{\partial Z_2}\left(\frac{1}{\xi}\frac{\partial\xi V_2}{\partial Z_2}\right)+\frac{\partial^2 V_2}{\partial Z_1^2}\right]+f_2 \tag{4.3}$$

where ρ is density, μ is molecular viscosity of fluid and P is static pressure in fluid. Body forces in directions Z_1 and Z_2 are designated by f_1 and f_2, respectively.

The buoyancy and the induced electromagnetic forces belong to the category of the body force appeared in the equations of motion. On the other hand, the shear stress caused by an impinging jet or a surface tension is introduced by boundary conditions.

For the convenience of computation, Eqs. (4.1) to (4.3) can be written in terms of the vorticity, ω, and the stream function, ψ, defined as:

$$\omega=\frac{\partial V_2}{\partial Z_1}-\frac{\partial V_1}{\partial Z_2} \tag{4.4}$$

$$V_2=-\frac{1}{\rho\xi}\frac{\partial\psi}{\partial Z_1} \tag{4.5}$$

$$V_1=\frac{1}{\rho\xi}\frac{\partial\psi}{\partial Z_2} \tag{4.6}$$

From Eqs. (4.2) and (4.3), we obtain the vorticity transport equation:

$$\xi^2\left\{\frac{\partial}{\partial Z_1}\left(\frac{\omega}{\xi}\frac{\partial\psi}{\partial Z_2}\right)-\frac{\partial}{\partial Z_2}\left(\frac{\omega}{\xi}\frac{\partial\psi}{\partial Z_1}\right)\right\}-\frac{\partial}{\partial Z_1}\left\{\xi^3\frac{\partial}{\partial Z_1}\left(\mu\frac{\omega}{\xi}\right)\right\}$$
$$-\frac{\partial}{\partial Z_2}\left\{\xi^3\frac{\partial}{\partial Z_2}\left(\mu\frac{\omega}{\xi}\right)\right\}+\xi^2\left(\frac{\partial f_1}{\partial Z_2}-\frac{\partial f_2}{\partial Z_1}\right)=0 \tag{4.7}$$

By combining Eqs. (4.4). (4.5) and (4.6), the stream function and the vorticity can be related by the following equation:

$$\frac{\partial}{\partial Z_1}\left(\frac{1}{\rho\xi}\frac{\xi\psi}{\partial Z_1}\right)+\frac{\partial}{\partial Z_2}\left(\frac{1}{\rho\xi}\frac{\partial\psi}{\partial Z_2}\right)+\omega=0 \tag{4.8}$$

Equations (4.7) and (4.8) may be applied to turbulent flow provided the molecular viscosity, μ, is substituted by the effective viscosity, μ_e. The effective viscosity is defined as

$$\mu_e=\mu+\mu_t \tag{4.9}$$

where the turbulent viscosity, μ_t, is not a physical property of the fluid but may be dependent on the position and structure of turbulence.

Since the development of an acceptable expression for μ_t is considered as a crucial factor in the mathematical model describing the turbulent flow system, a brief discussion on this problem is given below.

In the simplest formulation for the turbulent viscosity, the value of μ_t is maintained at a constant higher than that of the molecular viscosity.

Another expression for the turbulent viscosity is given as follows:

$$\mu_t=\rho K^{\frac{1}{2}}/l \tag{4.10}$$

where l is the length scale of turbulence for which an accurate value is not reported yet. The value of K can be quantitatively determined from the solution of the differential equation expressing the conservation of turbulent energy (so-called one-equation model).

Furthermore, the turbulent viscosity is also represented as follows:

$$\mu_t=\rho C_D K^2/\varepsilon \tag{4.11}$$

where C_D is a constant. In Eq. (4.11), both the turbulent energy, K, and the turbulent dissipation energy, ε, can be determined by using the solution of the respective differential equations concerning K and ε, (so-called two-equation model).

The length scale of turbulence is not involved in Eq. (4.11) and therefore two-equation model may be expected to be a more reliable procedure than one-equation model. It must be noted, however, that this additional reliability can be achieved at the expense of an increased computational labor.

The turbulent models were proposed by Spalding and his coworkers[1] who did pioneering works on the actual quantitative computation of the complex recirculating flow. The detailed discussion of the relative merits of these models were outlined by Launder, et al.[2].

Applications of these models to metal processing have been presented by Szekely and his coworkers.[3~5] Their interesting applications have been developed over a wide range, e. g., stirring and solidification of molten metal, and coalescence and floatation of inclusion particles.

The numerical computation of the three dimensional mathematical models of fluid flow, although available nowadays, is costly because of the excessively long computation time required. Moreover, the simulation to be obtained by such computation is apt to give comparatively approximate results. The problem especially arises in the case of turbulent flow in which the lack of experimental data renders the verification of the results difficult.

4. 2. Mixing Phenomena of Liquid Bath Stirred by Gas Injection

(1) Introduction

With regard to the concepts expressing the aspect of mixing, two kinds of technical terms have been extensively used hitherto in metallurgical processes. Namely, one is "mixing power density" which is a function of the operating conditions and the physical properties of the system, and the other is "mixing time", by which the rate of approach to the uniformity of system can be estimated. The relationship between these terms was proposed by Nakanishi and Fujii,[6] which enables us to evaluate the required flow rate of gas and the approximate degree of mixing.

In this section, the relations between the uniform mixing time, τ, and the mixing power density, ε, are analyzed from the viewpoint of transport phenomena, and the validities of the theoretical results are verified by cold model experiments for various types of metallurgical vessels.

(2) Relationship Between Flow Velocity and Mixing Power Density[7]

Navier-Stokes equation is applicable to both laminar and turbulent flows of a homogeneous fluid. Now, Eqs, (4. 2) and (4. 3) can be expressed as

$$\rho\left(\frac{\partial \bar{v}}{\partial t}+\bar{v}\cdot\nabla\bar{v}\right)=-\nabla P+\mu_e\nabla^2\bar{v}+\bar{F} \tag{4. 12}$$

where $\bar{F}$ refers to the body force and is generated by the injection of gas.

Focussing on the term involved in Eq. (4. 12) which competes with the magnitude of the body force, we classify the fluid motion as follows:

(i) Case where the viscous force predominates

From Eq. (4. 12), we can obtain as

$$\mu\nabla^2\bar{v}=-\bar{F} \tag{4. 13}$$

Now, it may be considered that the operator, ∇, in Eq. (4. 13) is in inverse proportion to the characteristic length, L. Thus, Eq. (4. 14) can be derived from Eq. (4. 13) on the basis of the procedure of the dimensional analysis.

$$v\propto(FL^2/\mu) \tag{4. 14}$$

where v is the characteristic velocity in the vessel.

(ii) Case where the inertia force predominates

We simplify Eq. (4. 12) as

$$\rho\bar{v}\cdot\nabla\bar{v}=\bar{F} \tag{4. 15}$$

Following the same manner as in the derivation of Eq. (4. 14), we can obtain as

$$v\propto(FL/\rho)^{\frac{1}{2}} \tag{4. 16}$$

(iii) Case where the turbulent viscous force predominates

We can write an equation similar to Eq. (4. 13), but μ has to be replaced by μ_t,

$$\mu_t\nabla^2\bar{v}=-\bar{F} \tag{4. 17}$$

From the Boussinesq and Prandtl hypothesis, the turbulent viscosity can be

expressed as

$$\mu_t = \rho l^2 |\text{grad } v| \tag{4.18}$$

Substituting Eq. (4.18) into Eq. (4.17) and adopting a procedure similar to the derivation of Eq. (4.14), we obtain

$$v \propto (FL^3/\rho l^2)^{\frac{1}{2}} \tag{4.19}$$

The mixing power density expresses the energy dissipated per unit time and per unit volume, and thus, the following relation may be written.

$$\varepsilon \propto F \cdot v \tag{4.20}$$

Applying Eq. (4.20) to Eqs. (4.14), (4.16) and (4.19), we can write the following relations between v and ε.

(i) Case where the viscous force predominates

$$v \propto (L^2\varepsilon/\mu)^{\frac{1}{2}} \tag{4.21}$$

(ii) Case where the inertia force predominates

$$v \propto (L\varepsilon/\rho)^{\frac{1}{3}} \tag{4.22}$$

(iii) Case where the turbulent viscous force predominates

$$v \propto (L^3\varepsilon/\rho l^2)^{\frac{1}{3}} \tag{4.23}$$

Now we can express the mass balance equation for a key component as Eq. (4.24),

$$\frac{\partial c}{\partial t} + \bar{v} \cdot \nabla c = D_e \nabla^2 c \tag{4.24}$$

On the basis of the predominant mechanism in the mass transfer, Eq. (4.24) can be simplified as in the following cases (A), (B) and (C).

(A) Case where the molecular diffusion predominates

In this case Eq. (4.24) reduces to the following equation.

$$\frac{\partial c}{\partial t} = D\nabla^2 c \tag{4.25}$$

For Eq. (4.25), we make an approximation with the following expression:

$$dC/dt = -kDC/L^2 \tag{4.26}$$

where k is a constant and C is the characteristic concentration.

By integrating Eq. (4.26), we obtain as

$$C \propto \exp(-kDt/L^2) \tag{4.27}$$

Now we suppose that the mixing time, τ, is the time elapsed till the value of C becomes invariant. Thus, by keeping the exponential power in the right-hand

side of Eq. (4.27) constant, we can write the following expression:

$$\tau \propto (L^2/D) \tag{4.28}$$

In practice, the mixing time is considered as the time when the concentration of the tracer falls in to a narrow range near the final concentration. The size of the range defined by researchers differs from one to another. It should be noted that it is meaningless to compare the values of the mixing times based on different definitions.

(B) Case where the convection predominates

In this case Eq. (4.24) is simplified as the following equation:

$$\frac{\partial c}{\partial t} = -\bar{v} \cdot \nabla c \tag{4.29}$$

Replacing $\bar{v}$ by the characteristic velocity, v, and adopting a procedure similar to Case (A) mentioned above, we write as

$$dC/dt = -kvC/L \tag{4.30}$$

Integrating Eq. (4.30), the following expression yields

$$C \propto \exp(-kvt/L) \tag{4.31}$$

Similarly, the mixing time may be described as

$$\tau \propto (L/v) \tag{4.32}$$

(C) Case where the turbulent diffusion predominates

In this case, the molecular diffusivity, D, in Eqs. (4.25) and (4.28) is replaced by the turbulent diffusivity, D_t. Thus, the mixing time in this case can be expressed as

$$\tau \propto (L^2/D_t) \tag{4.33}$$

Since the value of D_t can be regarded as large as the eddy kinematic viscosity[8], $\nu_t (=\mu_t/\rho)$, thus from Eq. (4.18) we have

$$D_t = l^2 |\mathrm{grad}\, v| \tag{4.34}$$

Combining Eq. (4.33) and Eq. (4.34), we obtain as

$$\tau \propto L^3/l^2 v \tag{4.35}$$

Equation (4.36) shows the effects of ε, L, l, ρ, μ and D upon τ in the specific case of combining the predominant force in fluid motion (i, ii, iii) and the predominant dispersion process in mass transfer (A, B, C).

$$\tau \propto \varepsilon^{-n} L^{\gamma} l^{\xi} \rho^{\alpha} \mu^{\beta} D^{\kappa} \tag{4.36}$$

It may be found that the mixing time in the case of combining (i) and (B) is independent of the characteristic vessel size ($\gamma = 0$) and is inversely proportional to the square root of the mixing power density ($n = 1/2$). Similarly, we can see that $n = 1/3$ and $\gamma + \xi = 2/3$ are given in the respective cases of combining (ii) & (B),

(iii) & (B), (ii) & (C) and (iii) & (C).

(3) Experimental Confirmation

The values of τ and v were measured through experiments conducted in the cylindrical vessels in which water was agitated by air blown from the center of the bottom. The diameter of the vessels were 0.405, 0.20 and 0.10 m, and the liquid depth was kept at a value equal to the diameter.

Experimencal results obtained from a vessel of 0.20 in diameter are shown in Fig. 4.1. It is found from Fig. 4.1 that there exists an inflection point at about $\varepsilon=8\mathrm{W/m^3}$, and that the relations between v and ε are shown as $v\propto\varepsilon^{0.48}$ and $v\propto\varepsilon^{0.25}$ on the left and right sides of the inflection point, respectively. On the other hand, the theoretical relations have been given as $v\propto\varepsilon^{1/2}$ and $v\propto\varepsilon^{1/3}$ from Eq. (4.21) and Eq. (4.22) or Eq. (4.23), respectively. Thus, it may be found that the measured values of the power of ε are nearly equal to the theoretical values.

Lehner, et al.[9] observed the surface velocities of molten steel agitated by argon gas in 60t-ladle at various radial positions and found that the surface velocity at any radial position was in proportion to the one-third power of the flow rate of gas. Since ε is approximately proportional to the flow rate of gas[7], the relation of $v\propto\varepsilon^{1/3}$ may be verified from the results observed by them.

Figure 4.2 shows the relations of τ and ε observed in the three vessels having different sizes. It may be seen from Fig. 4.2 that in the case in which the inertia force or the turbulent viscous force predominates the relation $\tau\propto L^{0.36}$ holds, but in the case in which the viscous force predominates τ is independent of L.

(4) Evaluation of Mixing Power Density

The equations for evaluating the value of ε are given as below:

(a) BOF process[10]

$$\varepsilon=3.95Q^3/(d^3hV_m)\quad(\mathrm{W/m^3}) \tag{4.37}$$

where d is the nozzle diameter, h is the distance between nozzle and metal surface and Q is the gas flow rate.

(b) RH degassing process

$$\varepsilon=Q_l\rho_l(u_l)^2/2V_m\quad(\mathrm{W/m^3}) \tag{4.38}$$

where Q_l and u_l are the flow rate ($\mathrm{m^3/s}$) and velocity of liquid in the down-leg,

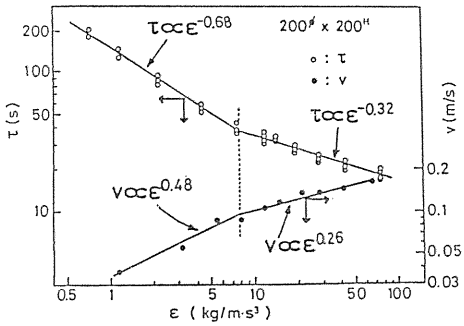

Fig. 4.1. Effect of mixing power density on mixing time and fluid velocity[7]. (case of $200^{\phi}\times200^{H}$)

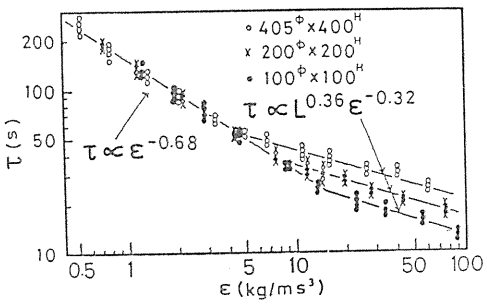

Fig. 4.2. Effect of vessel size on the relationship between mixing time and mixing power density[7].

respectively.

4. 3. Evaluation of Interfacial Area in Gas-Liquid System

(1) Introduction

On the gas-liquid reaction in the metallurgical processes, abundant literature has been reported hitherto. In these reactions, the evaluation of the interfacial area between gas and liquid phases becomes an important subject.

It is desirable that the empirical determinations of the mass transfer coefficient, k_l (m/s), and the volumetric interfacial area, a (m^2/m^3), should be handled independently. However, generally their product is obtained from the experiments concerning metallurgical processes.

Now, two techniques for measuring the interfacial area between gas phase and liquid phase are mainly adopted in the field of chemical engineering. One of these techniques which is chemical by nature employs the absorption process accompanied by reaction. The other technique being physical by nature utilizes optical properties of dispersion. However, in metallurgical fields, it is difficult to find out a reaction system which may be available for the former techinque, and for the latter one, a transparent liquid is required.

(2) Chemical Method of Measurement

The governing equation for a simultaneous absorption and reaction process can be described as follows:

$$D\frac{\partial^2 c}{\partial x^2}=\frac{\partial c}{\partial t}+r(c) \tag{4.39}$$

where $r(c)$ denotes the reaction rate and is a function of the concentration of the key component.

In the case where the reaction is fast enough to take place appreciably during the life of the surface elements of fluid, which appear on the gas-liquid interface from the bulk liquid, r (c) may be much larger than $(\partial c/\partial t)$. Thus, Eq. (4. 39) reduces to:

$$D\frac{\partial^2 c}{\partial x^2}=r(c) \tag{4.40}$$

The boundary conditions are as follows:

$$c=c_0 \qquad \text{at} \quad x=0 \tag{4.41}$$

$$dc/dx=0, \quad c=0 \qquad \text{at} \quad x=\infty \tag{4.42}$$

where c_0 is the concentration at interface.

Now, if a new variable β is introduced as

$$\beta=dc/dx \tag{4.43}$$

Equation (4. 40) can be reduced to Eq. (4. 44).

$$D\beta(d\beta/dc)=r(c) \tag{4.44}$$

The integral of Eq. (4. 44) satisfying Eq. (4. 42) is

$$D(\beta^2/2)=\int_0^C r(c)\,dc \tag{4.45}$$

It is seen from Eq. (4.43) that β denotes the concentration gradient and is an intrinsically negative variable, hence from Eqs. (4.43) and (4.45), we have

$$\frac{dc}{dx}=\beta=-\left\{\frac{2}{D}\int_0^C r(c)\,dc\right\}^{\frac{1}{2}} \tag{4.46}$$

Integrating Eq. (4.46) under the condition of $c=c$ at $x=x$, we obtain as

$$\int_C^{C_0}\frac{dc}{\{(2/D)\int_0^C r(c)\,dc\}^{\frac{1}{2}}}=x \tag{4.47}$$

Equation (4.47) gives the concentration distribution along the x-axis. Thus the absorption rate can be obtained directly from Eqs. (4.41) and (4.46).

$$V\equiv -D\beta_{x=0}=\{2D\int_0^{C_0} r(c)\,dc\}^{\frac{1}{2}} \tag{4.48}$$

where V is the mass flux at the interface.

Whatever the analytical form of $r(c)$, Eqs. (4.47) and (4.48) are available, and without adopting any special form for r (c) we can study the properties of a fast reaction succeeded to absorption process. In fact, we can conclude from Eq. (4.48) that in the case of a fast reaction, the absorption rate does not depend on the flow conditions of the liquid phase.

This conclusion becomes the basis of the method for the measurement of interfacial area.

Now, it may be assumed that $r(c)$ takes the form of the following expression:

$$r=k_n c^n \tag{4.49}$$

where k_n is the reaction rate constant.

Then, from Eqs. (4.48) and (4.49) we can obtain as

$$V=-D\frac{dc}{dx}\Big|_{x=0}=\left\{\left(\frac{2}{n+1}\right)Dk_n\right\}^{\frac{1}{2}}(c_0)^{(n+1)/2} \tag{4.50}$$

(3) Measurement of Interfacial Area

According to Eq. (4.50), the absorption rate in a fast reaction succeeded to absorption process is independent of the flow conditions. This concept can be applied to the measurement of interfacial area, provided the conditions described below are satisfied.

(a) Gas-phase resistance to the mass transfer is negligible.

(b) Absorption process takes place with a fast reaction.

Two kinds of absorption processes have been widely used for the measurement of interfacial area. Namely, these are, the process in which CO_2 gas is absorbed in NaOH aqueous solution and the one in which O_2 gas is absorbed in the sodium sulfite aqueous solution in the presence of a liquid-phase catalyst.

Yoshimatsu, et al.[11] applied the chemical method of measurement to a model experiment of the metallurgical process. They injected CO_2 gas into the bath of

NaOH aqueous solution from the bottom of a cylindrical vessel. Since the reaction system of CO_2-NaOH solution may be considered as a pseudo-first order, by putting $n=1$ in Eq. (4.50), we obtain

$$V=\sqrt{Dk_1}c_0 \tag{4.51}$$

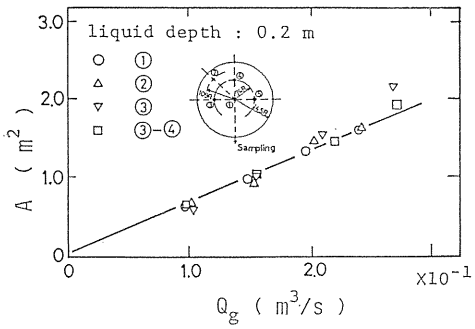

Fig. 4.3. The relation between the interfacial area and the gas blowing rate.

where k_1 is the reaction rate constant (1/s).

Figure 4.3 shows the the relation between the interfacial area, A (m^2) and the various blowing rates of gas, Q_g (m^3/s). Here, the interfacial area can be determined as

$$A=N/V \tag{4.52}$$

where N is the rate of absorption (kmol/s).

It is found from Fig. 4.3 that the interfacial area does not depend on the position of the injecting gas and A is in proportion to the blowing rate of gas.

Miller[12] reported the results of the experiments in which oxygen was absorbed in the sodium sulfite aqueous solution in the presence of cobaltous sulfate catalyst.

(4) Physical Method of Measurement

A beam of light passing through a dispersed system is deflected by obstacles. If we can select a suitable condition such that the deflected light can not reach the receiver, we can measure only the light which has not encountered an obstacle. This method was developed by Calderbank[13].

Landau, et al.[14] improved this method and proposed the following empirical equation:

$$I/I_0=\exp\{-6.59(1-e^{-0.0582\lambda a_D})\} \tag{4.53}$$

where I/I_0 is the transmitted fraction of light (−), λ is the optical path length (m) and a_D is the interfacial area per unit volume of the dispersed system (m^{-1}). Equation (4.53) is exactly applicable for the value of λa_D up to the order of 80.

Another physical method is to measure the distribution of bubble diameters by taking a photograph through the vessel.

When the distribution has been obtained, Sauter mean diameter, d_{SM} can be calculated from the following expression:

$$d_{SM}=\sum n_i d_i^3/\sum n_i d_i^2=6\alpha/a_D \tag{4.54}$$

where n_i is the number of bubbles having spherical diameter, d_i, of equivalent volume and α is the hold-up of the bubbles. Then, the interfacial area per unit volume of liquid phase, a (m^2/m^3), can be expressed as

$$a=6\alpha/\{(1-\alpha)d_{SM}\} \tag{4.55}$$

Nomenclature

A : interfacial area (m^2)
a_D : interfacial area per unit volume of the dispersed system (m^{-1})
C : characteristic concentration ($kmol/m^3$)
c : concentration ($kmol/m^3$)
c_D : constant (−)
c_0 : concentration at interface ($kmol/m^3$)
D : molecular diffusivity (m^2/s)
D_e : effective diffusivity (m^2/s)
d : nozzle diameter (m)
d_i : bubble diameter (m)
$\bar{F}$, F : body force (N/m^3)
f_1, f_2 : body force in directions Z_1 and Z_2 (N/m^3)
h : distance between nozzle and metal surface (m)
K : turbulent energy (m^2/s^2)
k : constant (−)
k_n : reaction rate constant ($(m^3/kg)^{n-1}/s$)
L : characteristic length (m)
l : length scale of turbulence (m)
N : rate of absorption (kmol/s)
n_i : number of bubbles having spherical diameter, d_i (−)
P : static pressure (Pa)
Q : gas flow rate (Nm^3/s)
Q_f : blowing rate of gas (m^3/s)
Q_l : metal flow rate (m^3/s)
r : reaction rate ($kmol/m^3s$)
t : time (s)
u_l : velocity of metal (m/s)
V : mass flux at interface ($kmol/m^2s$)
V_m : metal volume (m^3)
V_1, V_2 : velocity in direction Z_1 and Z_2 (m/s)
$\bar{V}$: velocity (m/s)
x : distance from gas-liquid interface (m)
Z_1 : axial or longitudinal coordinate (m)
Z_2 : radial or lateral coordinate (m)
α : hold-up of bubbles (−)
β : concentration gradient ($kmol/m^4$)
ε : turbulent dissipation energy (m^2/s^3), mixing power density (W/m^3)
λ : optical path length (m)
μ : molecular viscosity (Pa·s)
μ_e : effective viscosity (Pa·s)
μ_t : turbulent viscosity (Pa·s)
ρ : density (kg/m^3)
τ : mixing time (s)
ψ : stream function (kg/s)
ω : vorticity (1/s)

References

1) Gosman, A. D., Pun, W. M., Runchal, A. K., Spalding, D. B. and Wolfshtein, M., "Heat and Mass Transfer in Recirculating Flow", Academic Press, London and New York, (1969).
2) Launder, B. E. and Spalding, D. B., "Mathematical Models of Turbulence", Academic Press, London and New York, (1972).
3) Szekely, J., Lehner, T. and Chang, C. W., Ironmaking & Steelmaking, 6, 285 (1979).
4) Grevet, J. H., Szekely, J. and EL-Kaddah, N., Int. J. Heat Mass Transfer, 25, 487 (1982).
5) Szekely, J., Dilawari, A. H. and Metz, R., Met. Trans., 10B, 33 (1979).
6) Nakanishi, K. and Fujii, T., Tetsu-to-Hagané, 59, S460 (1973).
7) Asai, S., Okamoto, T., He, J. C. and Muchi, I., Trans. ISIJ, 23 (1) 43 (1983).
8) Katto, Y., "Dennetsugairon", Yōkendo, Tokyo, (1966).
9) Lehner, T., Carlsson, G. and Hsiao, T. C., SCANINJECT Ⅱ, 2nd Int'l. Conf. on Injection Metallurgy, MEFOS and Jernkontoret, Luleá, 22 (1980).
10) Emi, T., Nakanishi, K., Saito, K., Kato, Y., Nakamura, H. and Suzuki, K., The 19th Committee (Steelmaking), the Japan Society for the Promotion of Science, Report No. 10303 (1980).
11) Yoshimatsu, S. and Fukuzawa, A., Report Presented on the Meeting of Steel Refining Reaction Committee of ISIJ, (1983).
12) Miller, D. N., A. I. C*h*. E. Journal, 29, 312 (1983).
13) Calderbank, P. H., Trans. Instn. Chem. Engrs. (London), 36, 443 (1958).
14) Landau, J., Gomaa, H. G. and Al Tawell, A. M., Trans. Instn. Chem. Engrs. (London), 55, 212 (1977).

5. Mathematical Descriptions for Steelmaking Processes

5. 1. LD Converter

(1) Basic Concepts of the Model

The variations in the concentrations of the components present in the steel bath of *LD* converter caused by oxidation, may be determined by the balance of the two different tendencies namely, the one which allows the system to approach equilibrium, and the other caused by oxygen which is fed into the bath and keeps the system away from equilibrium.

In Fig. 5.1 (a), the solid line (1) represents the equilibrium line between $\underline{C}$ and $\underline{O}$ and the dotted line (2) shows the trajectory path along which $\underline{C}$ and $\underline{O}$ actually shift during refining.

In the first and second refining periods, a large part of oxygen is consumed by decarburization and the rest may be accumulated in the bulk of molten steel. Taking the mass balance for oxygen at any elapsed time of blowing, θ, Eq. (5.1) can be obtained:

$$\int_0^{\theta} (s/w)\, d\theta = (C_o - C_{i,o}) + (M_o/M_c)\,(C_{i,c} - C_c) \qquad (5.1)$$

Equation (5.1) represents the operating line (3) which moves in the direction of the arrow as θ increases. If the feeding of oxygen is ceased at the moment when

the concentrations of carbon and oxygen are showen by point J, then this point moves toward M along the path of the operating line (3), and finally the system reaches its equilibrium state at point M. Since the epuilibrium relation between $\underline{C}$ and $\underline{O}$ can be expressed as Eq. (5. 2), the intersection of the operating and equilibrium lines can be determined by Eqs. (5. 1) and (5. 2) as a function of the elapsed time of blowing, the temperature of molten steel and the partial pressure of carbon monoxide.

$$C_O \cdot C_C = P_{CO}/K(T) \qquad (5.2)$$

If the concentrations of carbon and oxygen are shown by point L and the intersection of the operating and equilibrium lines is given by point N which has the coordinates (C_C^*, C_O^*), then the system moves from L to N by the driving force $\overrightarrow{LN}$.

Figure 5. 1 (b) is a magnified figure of Fig. 5. 1 (a), The driving force, $\overrightarrow{LN}$, can be resolved into the two driving forces $\overrightarrow{LO}$ and $\overrightarrow{LP}$. The smaller the resistance of mass transfer is, the more rapidly the system moves toward the point N.

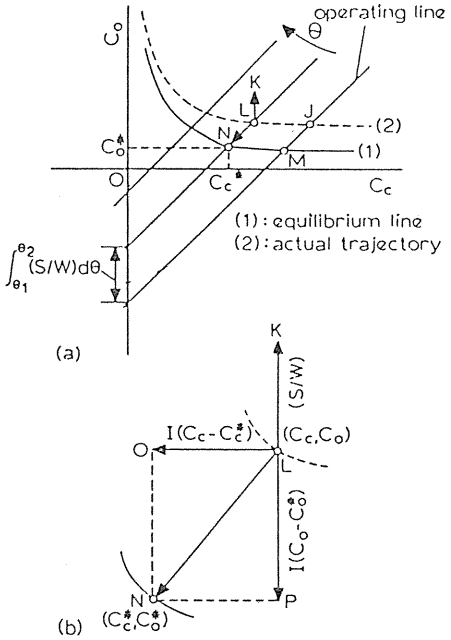

Fig. 5. 1.
(a) Relations between the concentrations of carbon and oxygen in molten steel and the operating line.
(b) Illustration of the driving force.

As is shown by dotted line in Fig. 5. 1 (a), the actual relation of $\underline{C}$ and $\underline{O}$ found in practical operations can be determined from the driving force $\overrightarrow{LN}$ and the resistance of mass transfer. The driving force $\overrightarrow{LN}$ increases the increase in the moving rate of the operating line which can be controlled by the feeding rate of oxygen.

The resistance of mass transfer may be connected with the circulating flow rate of molten steel in the bath (or mixing intensity) as will be discussed later.

From the considerations mentioned above, the difference in oxygen level among the experimental data obtained from open-hearth, LD converter and crucible can be explained as follows. Examining the experimental data[1] reported hitherto, the largest gap between the observed and equilibrium oxygen levels can be seen in open-hearth and the second in LD converter. The data obtained from crucible almost coincide with equilibrium.

In open-hearth, because of the low feeding rate of oxygen, the driving force, $\overrightarrow{LN}$, is small. Moreover, the mixing intensity may be very weak. Hence, the balance of the driving force and the mixing intensity may produce the largest deviation from equilibrium.

In the case of LD converter, though the feeding rate of oxygen is very large, the mixing intensity is also remarkable. Consequently, it may be inferred that the

data of *LD* converter are located more close to equilibrium than those of open-hearth.

In the case of crucible experiments using an induction furnace, the feeding rate of oxygen is very low. On the other hand, the mixing intensity induced by electromagnetic force is striking. Thereby, the data of crucible may closely approach to the equilibrium line.

On the basis of the above considerations, the governing equations of the concentrations of $\underline{C}$ and $\underline{O}$ can be expressed as Eqs. (5. 3) and (5. 4)

$$dC_c/d\theta = I(C_c^* - C_c) \tag{5.3}$$

$$dC_o/d\theta = I(C_o^* - C_o) \tag{5.4}$$

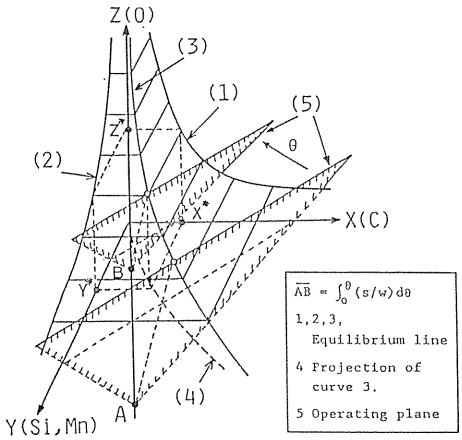

Fig. 5. 2. Schematic diagram of the equilibrium operating planes given in rectangular coordinates.

where the position (C_c^*, C_o^*) corresponds to that of point N in Fig. 5. 1 and I denotes the inverse of the mass transfer resistance.

In Fig. 5. 2, the concentration relations of $\underline{C}$-$\underline{Si}$-$\underline{O}$ and $\underline{C}$-$\underline{Mn}$-$\underline{O}$ systems are illustrated in the rectangular coordinates (X, Y, Z). The coordinate axes, X, Y, and Z denote the concentrations of $\underline{C}$, $\underline{Si}$ or $\underline{Mn}$ and $\underline{O}$, respectively. The equilibrium lines of X to Z and Y to Z are illustrated by curve 1 on X-Z plane and curve 2 on Y-Z plane, respectively, and each equilibrium line forms a curved plane parallel to the Y- and X- axes, respectively. The intersection of these planes is the equilibrium line, i. e., curve 3 in three-dimensional system. Under the equilibrium state, the concentration relation of each component should be represented by this curve.

Taking the mass balance for oxygen in the ternary system ($\underline{C}$-$\underline{Si}$-$\underline{O}$), Eq, (5. 5) can be obtained.

$$\int_0^\theta (s/w)\,d\theta = (C_o - C_{i,\,o}) + (M_o/M_c)(C_{i,\,c} - C_c) + 2(M_o/M_{si})(C_{i,\,si} - C_{si}) \tag{5.5}$$

As is shown in Fig. 5. 2, Eq. (5. 5) represents the operating plane moving in the direction of the arrow as θ increases. In the same manner as the case of binary system, the transisional path of the system is driven toward the point where the operating plane and the equilibrium line intersect.

(2) Modelling

Based on the general concepts of the oxidation process mentioned above, a simplified model for *LD* converter is proposed, paying a special attention to the effects of the feeding rate of oxygen and the degree of mixing of molten steel on the transitional variations of composition.

Now, the following assumptions are adopted.

(i) Bath is divided into the reaction zone (i, e., a hot spot) and the bulk of steel as is shown by Fig. 5. 3.

(ii) Each component of steel flowed into the reaction zone instantaneously arrives at an equilibrium state due to the reaction with the absorbed oxygen, and then discharges from the reaction zone.

(iii) The discharged molten steel circulates again into the reaction zone after being completely mixed with bulk steel in the bath.

(iv) Since the accumulation of any component in the reaction zone is small in comparison with the bulk steel itself, it may be neglected.

(v) Carbon depletion by dissolution or other effects of scrap is neglected.

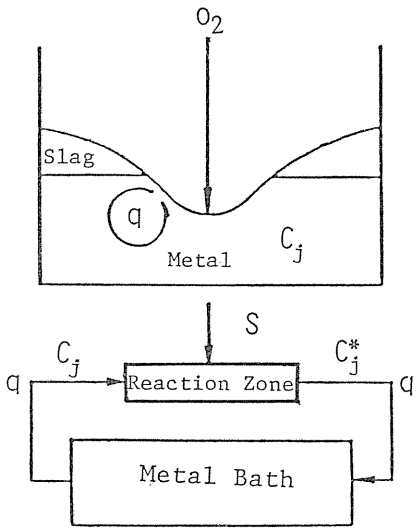

Fig. 5. 3. Schematic drawing of the concept of the mathematical model.

The relation between the concentration of the j-th component flowing into the reaction zone, C_j, and that of the same component discharging from the zone, C_j^*, is obtained as Eq. (5. 6)

$$w\{dC_j(t)/dt\}=q\{C_j^*(t)-C_j(t)\} \tag{5.6}$$

Focussing on the initial stages of refining, the reactions in the reaction zone are considered as follows

$$\underline{C}+\underline{O}\rightleftarrows CO(g) \tag{5.7}$$

$$\underline{Si}+2\underline{O}\rightleftarrows SiO_2 \tag{5.8}$$

To consider both of the oxidation reactions given in Eqs. (5. 7) and (5. 8), Eq. (5. 9) should be added to Eqs. (5. 3) and (5. 4)

$$dC_{Si}/d\theta=I(C_{Si}^*-C_{Si}) \tag{5.9}$$

The equilibrium relations between the i-th component in the systems of Eqs. (5. 7) and (5. 8) and oxygen are known as a function of temperature[2].

$$K_i=f(C_i,\ C_o,\ T) \tag{5.10}$$

Taking the mass balance for oxygen in the reaction zone in which each component is in equilibrium with oxygen, we obtain as

$$s+q(C_o-C_o^*)=q[(M_o/M_c)(C_c-C_c^*)+2(M_o/M_{Si})(C_{Si}-C_{Si}^*)] \tag{5.11}$$

Let us prove that Eq. (5. 11) is mathematically equivalent to Eq. (5. 5). Substituting Eqs. (5. 3), (5. 4) and (5. 9) into Eq. (5. 11), we obtain as

$$s+(q/I)(-dC_o/d\theta)=(q/I)(M_o/M_c)(-dC_c/d\theta)$$
$$+2(q/I)(M_o/M_{si})(-dC_{si}/d\theta) \quad (5.12)$$

Integrating Eq. (5.12), yields Eq. (5.13) which can be found to be equivalent to Eq. (5.5), if $I=q/w$ holds.

$$\int_0^\theta s d\theta=(q/I)(C_o-C_{i,o})+(M_o/M_c)(q/I)(C_{i,c}-C_c)$$
$$+2(M_o/M_{si})(q/I)(C_{i,si}-C_{si}) \quad (5.13)$$

Thus, it is noticed that the basic concepts of the model mentioned in section (1) are physically reflected in the assumptions (i)～(v) in this section. Furthermore, I, which was introduced in section (1), is found to be the circulating flow rate of molten steel per unit volume.

To extend the mathematical model from the initial stage to the middle stage of refining process, the reaction $Fe+\underline{O}=FeO$ should be considered and Eq. (5.11) is modified as Eq. (5.14)

$$s+q(C_o-C_o^*)=q[(M_o/M_c)(C_c-C_c^*)+2(M_o/M_{si})$$
$$(C_{si}-C_{si}^*)]+(M_o/M_{FeO})Q_{FeO} \quad (5.14)$$

Substituting Eq. (5.10) and the relation[3] between a_{SiO_2} and a_{FeO} given in the phase diagram of $a_{SiO_2}-a_{FeO}$[2] into Eq. (5.14), a polynominal function of C_o^* is obtained, and the function should be solved for C_o^*. Then substituting C_o^* into Eq. (5.10), $C_j^*(t)$ $(j=C, Si)$ can be calculated. Thus, substituting $C_j^*(t)$ into Eq. (5.6), $C_j(t+\Delta t)$ can be obtained. Repeating this procedure, the variation of C_j with time can be estimated.

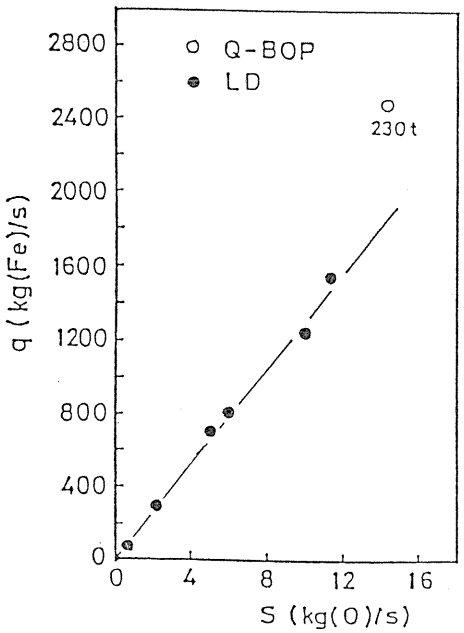

Fig. 5.4. The relation between circulating flow rate and gas blowing rate.

The only parameter which appears in this model is the circulating flow rate of molten steel, q. By selecting a suitable value for q, the variations of concentration were computed and fairly good agreement was obtained between the predictions of the model and the observed data[3]. Figure 5.4 shows the relation between the value of q adopted in calculation and the flow rate of oxygen, s, which is one of the operating conditions. The results obtained from *LD* converters of different capacity have shown that there exists a linear relation between q and s. However, the calculated values for Q-BOP deviates above the straight line for *LD* converter. This infers that the circulating flow rate of Q-BOP is larger than that of *LD* converter under the same feeding rate of

oxygen gas.

5. 2. Ladle Furnace

(1) Introduction

The ladle refining process is drawing attention due to the growing demand for high grade steel and the spreading of hot metal pretreatment. Theoretical and experimental approaches have been developed to improve the refining operations in the field of ladle metallurgy.

In the previous section (4. 2), the relationship between the mixing time and the mixing power density was derived on the basis of the procedure of dimensional analysis. In this section, a more precise approach for determining the mixing quality is given by using the rate of decrease in the fluctuation of concentration. The recycling model related to the mixing rate is developed by use of the transfer function. Furthermore, a mathematical model based on the operating conditions for evaluation of the recirculating flow rate is developed.

(2) Transfer Function for Recycle Mixing Model

(a) Tanks-in-Series Model

Here, we introduce the tanks-in-series model which is widely used to represent nonideal flow. We consider the fluid flow through a series of equal-size ideal stirred tanks. For large N, a residence time distribution (RTD) approaches to that of plug flow, and the mixing condition is complete when $N=1$. Thus, the only parameter of this model is the number of tanks in the chain. If we introduce a δ signal into the N-th stage system as shown in Fig. 5. 5, the recorder will measure the tracer as it flows by the first time, the second time, and so on. The output response is the superposition of all these signals.

The trasfer function of an ideal stirred tank can be expressed as

$$g(s)=1/\{(t_c s/N)+1\} \tag{5.15}$$

where s is an operator of Laplace transformation, $t_c=V/Q_l$ is the circulation time of fluid and N is the number of tanks. Then, the transfer function for a series of N tanks, $F(s)$, is expressed as

$$F(s)=[g(s)]^N=1/\{(t_c s/N)+1\}^N \tag{5.16}$$

If we introduce a δ-signal into a closed system where the output signal of the N-th tank is connected with the input signal of the first tank, the total transfer function, $Y(s)$, can be written as Eq. (5. 17)

$$\frac{Y(s)}{t_c}=\frac{F(s)}{1-F(s)}=\frac{1}{\{(t_c s/N)+1\}^N-1} \tag{5.17}$$

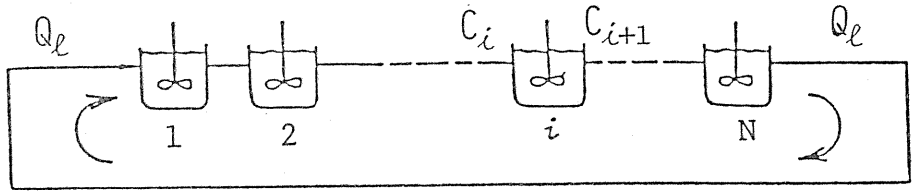

Fig. 5. 5. δ-input signal into a multistage closed system.
(number of stage: $i=1, 2, \ldots, N$)

Inverting Eq. (5.17), for large T, the impulse response for a recycle system becomes[19]

$$y(t)=1+2\exp(-2\pi^2 t/Nt_c)\cos\{2\pi t/t_c+2\pi/N\} \tag{5.18}$$

Equation (5.18) represents a sinusoidal wave with the decaying amplitude, A. The variance of $y(t)$ over one period, σ^2, is found as Eq. (5.19).[4]

$$\sigma^2=(t_c)^2/N=(\sigma_c t_c)^2 \tag{5.19}$$

Then, the decaying amplitude is given as:

$$A=2\exp\{-2\pi^2(\sigma_c)^2 t/t_c\} \tag{5.20}$$

(b) Experimental Results and Discussion

Maruyama et al.[5] conducted impulse response experiments to measure the mean circulation time. Figure 5.6 shows an example of the impulse response in which damping oscillation appears. Figure 5.7 shows a typical series of decaying amplitude as a function of time. The decay of amplitude is independent of the tracer injecting position and also of the measuring position, and it can be correlated by the solid line representing the theoretical prediction given by Eq. (5.20).

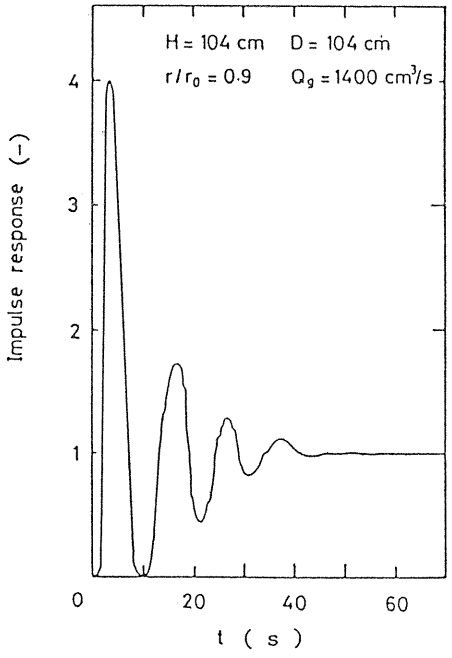

Fig. 5. 6. Typical example of impulse response for bubble-plume mixing. (By the courtesty of Maruyama et al.[5])

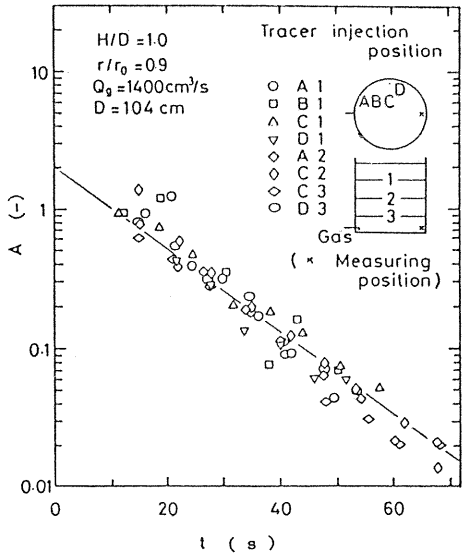

Fig. 5. 7. Amplitude, A, as a function of time. (By the courtesy of Maruyama et al.[5])

(3) Mathematical Model of the Gas-blown Ladle

(a) Mathematical Formulation

A quantitative macroscopic model and a sophisticated microscopic model developed by employing partial differential equations were presented by Sahai and Guthrie.[6,7]

An intermediate lumped model[8] described by ordinary differential equations is presented in the followings. The concept of the model is schematically shown in Fig. 5. 8. The bath is divided into three zones, i. e., the plume zone where bubbles rise into the stream of liquid, the ejecting flow zone where liquid exhausted from the plume zone is assumed to have only the radial velocity component, and the descending flow zone in which liquid flows downward. The liquid velocities in each zone are assumed to be uniform.

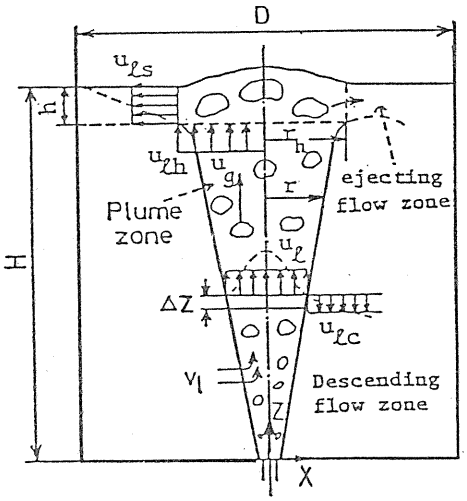

Fig. 5. 8. Schematic view of bottom blown vessel.

Taking the mass balances of gas and liquid in a differential element ΔZ in the plume zone yields Eqs. (5. 21) and (5. 22)

(for gas) $$M_g=\int_0^r \rho_g u_g \phi 2\pi x\, dx \tag{5.21}$$

(for liquid) $$(d/dZ)\int_0^r (1-\phi)\rho_l u_l 2\pi x\, dx=(2\pi x\rho_l u_l)_{x=r} \tag{5.22}$$

The momentum balance equation is given by Eq. (5. 23)

$$\int_0^r g\phi(\rho_l-\rho_g)2\pi x\, dx=(d/dZ)\int_0^r (1-\phi)\rho_l (u_l)^2 2\pi x\, dx \tag{5.23}$$

The term $(2\pi x\rho_l u_l)_{x=r}$ appearing in Eq. (5. 22) is the mass flow rate of the liquid entrained in the plume zone from the descending flow zone. The entrainment rate is assumed to be in proportion to the relative velocity and the interfacial area between the plume and the descending flow zones.

$$(2\pi x\rho_l u_l)_{x=r}=E_0\{2\pi r\rho_l(1-\phi)(u_l+u_{lc})\} \tag{5.24}$$

The mean velocity u_{lc} in the descending flow zone is determined by the over-all mass balance in the horizontal cross section.

$$\int_0^r u_l\rho_l(1-\phi)2\pi x\, dx=\int_r^{D/2} u_{lc}\rho_l 2\pi x\, dx \tag{5.25}$$

The slip velocity, u_s, being defined as Eq. (5. 26)

$$u_s=u_g-u_l \tag{5.26}$$

can be expressed as a function of the gas hold-up ϕ and the ascending velocity of

a single bubble, u_b, in the form[9]

$$u_s=u_b/(1-\phi) \tag{5.27}$$

The bubble diameter can be evaluated by Eq. (5.28) which is obtained by Davidson and Amick[10].

$$d_{bo}=0.569(Q_g d_n{}^{0.5})^{0.289} \tag{5.28}$$

The bubble volume during ascending can be expressed using the ideal gas law

$$V_b=V_{bo}\frac{p_s+H\rho_l g}{p_s+(H-Z)\rho_l g} \tag{5.29}$$

where V_{bo} is the initial bubble volume introduced from an orifice and is given as $V_{bo}=(1/6)\pi(\mathrm{d}_{bo})^3$. If no interaction between the dispersed bubbles is assumed, u_b as the ascending velocity of a single bubble is given by Eq. (5.30)

$$u_b=\sqrt{0.5d_b g} \tag{5.30}$$

The density of gas is based on the ideal gas law.

$$\rho_g=\rho_{gs}\frac{p_s+(H-Z)\rho_l g}{p_s} \tag{5.31}$$

Substituting Eqs. (5.24) to (5.31) into Eqs. (5.21) to (5.23) and rearranging, the first order differential equations regarding u_l, r and ϕ in the plume zone are obtained.

$$\frac{du_l}{dZ}=\frac{g\phi}{(1-\phi)u_l}-\frac{2E_o(R^2-\phi r^2)u_l}{r(R^2-r^2)} \tag{5.32}$$

$$\frac{dr}{dZ}=\frac{1}{2(u_l+u_s)}\left\{\frac{2E_o(R^2-\phi r^2)u_l}{R^2-r^2}-\frac{g\phi r}{(1-\phi)u_l}\right.$$
$$\left.-\frac{u_{bo}(k_1/k_2)^{1/6}r}{(1-\phi)^2}F(u_l,\ r,\ \phi,\ Z)+\frac{gr\rho_l u_{bo}(k_1/k_2)^{1/6}}{6(1-\phi)k_2}\right\}$$
$$-\frac{r}{2\phi}F(u_l,\ r,\ \phi,\ Z)+\frac{g\rho_l\rho_{gs}r}{2\rho_g p_s} \tag{5.33}$$

$$\frac{d\phi}{dZ}=F(u_l,\ r,\ \phi,\ Z)\equiv\left\{\frac{g\rho_l\rho_{gs}(1-\phi)}{p_s\rho_g}(u_l+u_s)\right.$$
$$-\frac{2E_o(1-\phi)(R^2-\phi r^2)}{r(R^2-r^2)}(u_l+2u_s)-\frac{g\phi u_s}{u_l^2}+\left.\frac{g\rho_l u_{bo}(k_1/k_2)^{1/6}}{6k_2}\right\}\Big/$$
$$\left\{\frac{(u_l+u_s)}{\phi}+\frac{u_{bo}(k_1/k_2)^{1/6}}{1-\phi}\right\} \tag{5.34}$$

where $k_1\equiv p_s+H\rho_l g$, $k_2\equiv p_s+(H-Z)\rho_l g$, $u_{bo}\equiv\sqrt{0.5d_{bo}g}$.

Since Eqs. (5.32) to (5.34) do not hold in the ejecting flow zone, another

approach will be required. Taking the mass balance in the ejecting flow zone, we obtain

$$u_{lh}\pi(r_h)^2\rho_l(1-\phi_h)=2\pi r_h h u_{ls}\rho_l \tag{5.35}$$

Equation(5.35) shows the balance between the vertical input from the horizontal plane at $Z=H-h$ and the radial output at $r=r_h$. Based on the energy balance, we can write as

$$\int_0^{r_h}(1-\phi_h)\rho_l\pi x(u_{lh})^3dx+\int_0^{r_h}\phi_h\rho_g\pi x(u_{gh})^3dx$$
$$=\pi r_h h\rho_l(u_{ls})^3+\int_0^h u_{ls}\rho_l 2\pi r_h g Z'dZ' \tag{5.36}$$

where $Z'=Z-(H-h)$.

The computing procedure is to calculate Eqs. (5.32) to (5.34) simultaneously from $Z=0$ to $Z=H-h$, where h is determined to satisfy Eqs. (5.35) and (5.36). By using the values of r_h, u_{lh} and ϕ_h at $Z=H-h$, the liquid flow rate, Q_l, can be calculated by the following equation.

$$Q_l=\pi(r_h)^2u_{lh}(1-\phi_h) \tag{5.37}$$

(b) Results and Discussion

One of the calculated results is shown in Fig. 5.9. Along the upward direction, the radius of the plume increases and the liquid velocity and the gas hold-up decrease.

Figure 5.10 shows the effects of liquid depth on the circulation flow rate. The solid lines predict the results calculated by use of the present mathematical model. The observed values were obtained from the experiments, in which the method of pursuing a tracer particle was adopted[8].

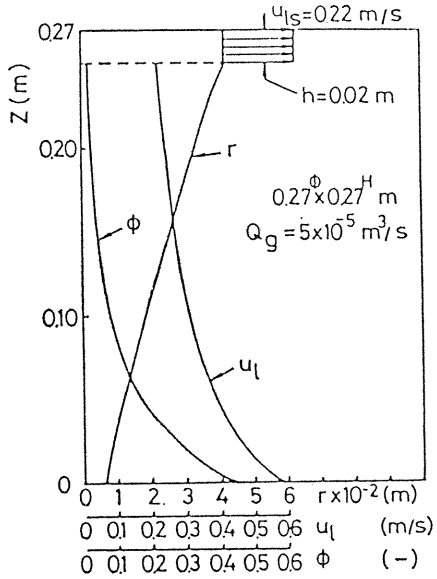

Fig. 5. 9. Calculated results of the longitudinal distribution of process variables.

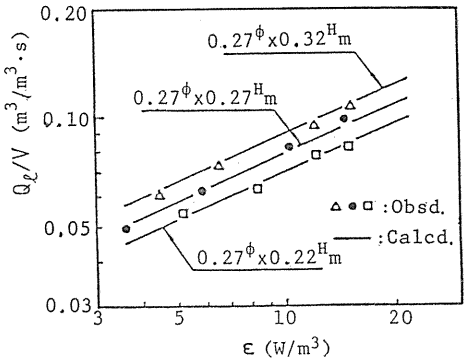

Fig. 5. 10. Effect of liquid height on the relation between circulation flow rate and applied power density.

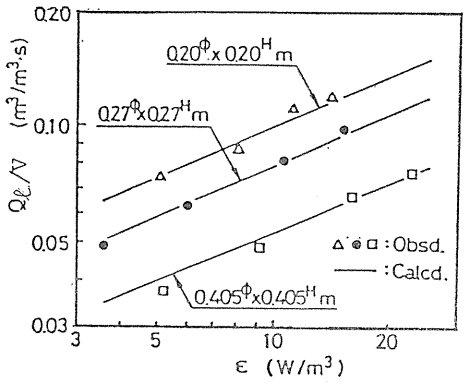

Fig. 5. 11. Effects of vessel size on the relation between circulation flow rate and applied power density.

The agreement between the calculated results and the observed data is fairly good. With increase of liquid depth. the recirculating flow rate per unit volume of liquid is increased under the same mixing power density.

Figure 5. 11 shows the effects of vessel size on circulation flow rate. It is found that the mathematical model can fairly predict the experimental data.

5. 3. RH Degassing Vessel

(1) Introduction

The degassing rate in *RH* process is mainly determined by one of the following three processes, i. e., the degassing process by an inert gas bubble injected into the up-leg, the free surface of molten steel in vacuum chamber, and the splash of molten steel in vacuum chamber. Concerning the first process, a mathematical model for the degassing in a two-phase flow is developed[11].

(2) Mathematical Model

To develop the mathematical model, the following assumptions are adopted.

(i) The flows of both the gas phase and the liquid phase in the up-leg are piston-type flows.

(ii) No bubble coarsening takes place in the up-leg and the shape of a bubble is spherical.

(iii) The rate controlling step in the degassing process is the mass transfer in the side of liquid phase.

On the basis of these assumptions, the following mass balance equations for C, O and H in molten steel can be written.

$$dC_{lC}/dZ = -k_{lC}Aa(C_{lC}-c^i_{lC})/Q_l \tag{5. 38}$$

$$dC_{lO}/dZ = -k_{lO}Aa(C_{lO}-C^i_{lO})/Q_l \tag{5. 39}$$

$$dC_{lH}/dZ = -k_{lH}Aa(C_{lH}-C^i_{lH})/Q_l \tag{5. 40}$$

where C_{lk} and C^i_{lk} are the bulk and interface concentrations of k-component in steel, k_{lk} is the mass transfer coefficient of k-component in molten steel, A is the cross sectional area of the up-leg and Q_l is the recirculating flow rate of liquid, a is the interfacial area per unit volume of the ascending two-phase and is given as follows:

$$a = 6Q_g/DA(u_l+u_r) \tag{5. 41}$$

where u_l is the ascending velocity of molten steel, D is a diameter of bubble and u_r is the relative velocity of a bubble.

On the other hand, Eqs. (5.42) and (5.43) are derived from the respective mass balances for H_2 and CO in a bubble.

$$dC_{gH}/dZ = k_{lH}Aa(C_{lH}-C^i_{lH})/2Q_g - (C_{gH}/Q_g)(dQ_g/dZ) \quad (5.42)$$

$$dC_{gCO}/dZ = k_{lC}Aa(C_{lC}-C^i_{lC})/Q_g - (C_{gCO}/Q_g)(dQ_g/dZ) \quad (5.43)$$

where C_{gj} is the concentration of j-component in a bubble, Q_g is the volumetric flow rate of rising bubble.

The equation of continuity in the two-phase flow can be written as

$$Q_l/u_l + Q_g/(u_l+u_r) = A \quad (5.44)$$

It has been reported that u_r is a function of u_l, the ratio of the volumetric flow rate of steel to that of gas and the diameter of a bubble[12,13]. Here. u_r is expressed as

$$u_r = B\sqrt{D} \quad (5.45)$$

where B is a constant.

Differentiating Eq. (5.44) with respect to Z and substituting Eq. (5.45) into the resulting equation and using the relation of $(Q_g/Q_g^\circ)^{1/3} = D/D^\circ$, (where D° and Q_g° are the bubble diameter and the gas flow rate at the point the gas is injected, respectively.), Eq. (5.46) is obtained.

$$(2Au_l - Q_l - Q_g + AB\sqrt{D})(du_l/dZ) - u_l(dQ_g/dZ) + (B/2\sqrt{D})(Au_l - Q_l)(dD/dZ) = 0 \quad (5.46)$$

To calculate the circulating flow rate, the pressure drop in the up-leg should be evaluated. Regarding the pressure drop in the two-phase flow, a number of theoretical and experimentical works have been conducted hitherto. Here, the theory of Stenning et al.[14] is introduced.

To take the momentum balance in the up-leg, let us take into account the gravitational force, F_g, the force due to pressure, F_p, and the friction force, F_f,as external forces.

$$F_g = -A\rho_l g(1-\varepsilon)dZ \quad (5.47)$$

$$F_p = -AdP \quad (5.48)$$

$$F_f = -(1/2)\rho_l(u_l)^2\pi D_u f dZ \quad (5.49)$$

where ρ_l is the density of liquid, g is the gravitational acceleration, D_u is the inner diameter of the up-leg, f is the friction factor at the wall of the up-leg and ε is the void fraction in the two-phase flow and is equivalent to the volumetric bubble ratio.

$$\varepsilon = Q_g/A(u_l+u_r) \quad (5.50)$$

The effective buoyancy force is expressed as Eq. (5.51).

$$F_b = A\varepsilon(\rho_l - \rho_g)gdZ \fallingdotseq A\varepsilon\rho_l gdZ \tag{5.51}$$

where ρ_g is the density of gas.

The difference between the input and the output momenta in the differential length dZ can be written as Eq. (5.52).

$$\begin{aligned} dm &= A(u_l)^2\rho_l(1-\varepsilon) - A(1-\varepsilon-d\varepsilon)(u_l+du_l)^2\rho_l \\ &= -A\rho_l d\{(1-\varepsilon)(u_l)^2\} \end{aligned} \tag{5.52}$$

By using Eqs. (5.47) to (5.52) the equation of motion for molten steel is given as Eq. (5.53).

$$\begin{aligned} &Q_l\rho_l(du_l/dZ) + A\rho_l g(1-2\varepsilon) + A(dP/dZ) \\ &\quad + (1/2)\rho_l(u_l)^2\pi D_u f = 0 \end{aligned} \tag{5.53}$$

The pressure in a bubble can be determined from the ideal gas law.

$$P = (C_{gi} + C_{gCO} + C_{gH})RT_g \tag{5.54}$$

where T_g is gas temperature and R is gas constant. Differentiating Eq. (5.54) with respect to Z and substituting Eqs. (5.42) and (5.43) into the resulting equation, Eq. (5.55) is obtained.

$$\frac{dP}{dZ} = \frac{RT_g aA}{Q_g}\left\{\frac{k_{lH}}{2}(C_{lH} - C^i_{lH}) + k_{lC}(C_{lC} - C^i_{lC})\right\} - \frac{P}{Q_g}\cdot\frac{dQ_g}{dZ} \tag{5.55}$$

By solving the simultaneous ordinary differential equations ((5.38) to (5.40), (5.42), (5.43), (5.46), (5.53), (5.55)), the circulating flow rate of molten steel and the degassing rate in the up-leg can be obtained.

(3) Calculated Results

The rising bubble grows in volume along the longitudinal direction due to the decrease in pressure and the mass transfer from molten steel. The circulating flow rate increases with the increase in the rising velocity of bubbles. On the basis of the mathematical model mentioned above, the longitudinal distributions of the process variables in the two-phase flow and the circulation flow rate of molten steel, Q_l, can be evaluated.

Figure 5.12 shows the longitudinal distribution of the process variables under the flow of an injected inert gas, of the rate 140 Nl/min. The vertical axis indicates the dimensionless distance in the up-leg measured from the blowing point at which the inert gas is injected. The dimensionless concentrations of CO and H_2 in a bubble are expressed on the basis of the equilibrium concentration of each gas. The diameter of a bubble, D^*, and the concentration of each component in molten steel, C_{lk} ($k=C, H, O$), are shown in dimensionless form by use of an initial bubble size and the value of the concentration of the respective component at the point the gas is injected.

The relation between Q_l and the injecting flow rate of inert gas, Q_g°, is shown in Fig. 5.13. The calculated results of Q_l are reasonable in comparison with the data reported by several investigators[15~17].

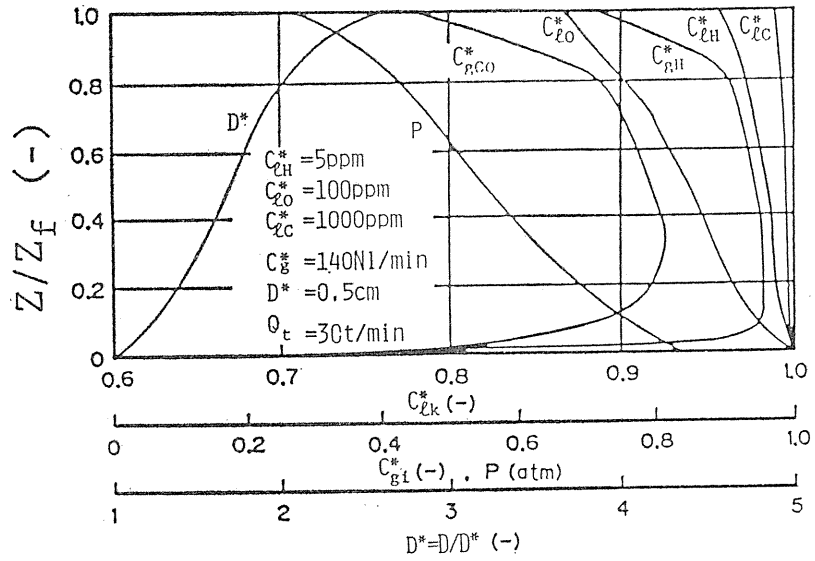

Fig. 5. 12. Calculated results of the longitudinal distribution of process variables in up-leg, where Q_g°=140 Nl/min.

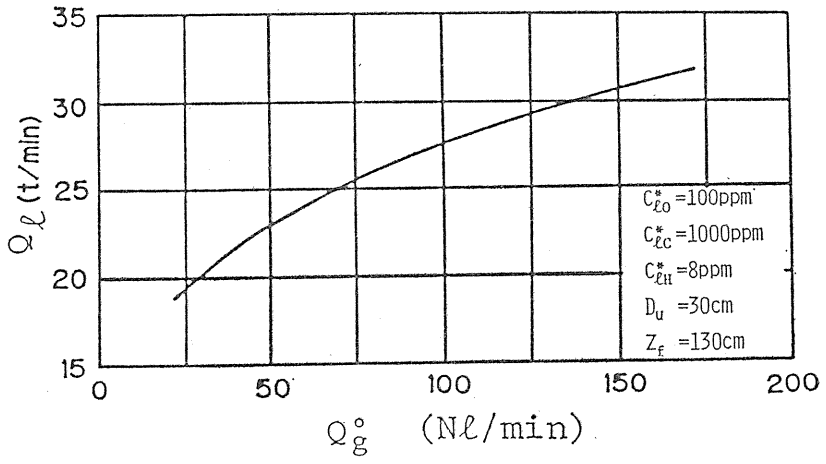

Fig. 5. 13. Relation between circulation-flow rate of molten steel Q_l and blowing rate of inert gas Q_g°.

5. 4. Stream Drop Degassing Vessel

In stream drop degassing process, it has been known that when the diameter of molten steel drop is less than 1 mm, the effect of the absolute pressure in a vacuum tank of the degassing vessel on the degassing efficiency becomes small. Now we consider the quantitative relationship between the drop size and the final concentration of a key component in a drop.

By taking the mass balance for hydrogen as the key component around a differential shell in a spherical drop, we obtain Eq. (5. 56)

$$\frac{\partial C}{\partial \theta}=D\left(\frac{\partial^2 C}{\partial r^2}+\frac{2}{r}\frac{\partial C}{\partial r}\right) \tag{5.56}$$

where C is the concentration of hydrogen, D is the molecular diffusivity, r is the radial position in the drop and θ is time.

The initial and boundary conditions are as follows:

$$C=C_i \quad \text{at} \quad \theta=0, \quad r\geq 0$$

$$C=C^* \quad \text{at} \quad r=r_0, \quad \theta>0$$

$$C \text{ is finite } (C<C_i) \quad \text{at} \quad r=0, \quad \theta>0$$

where C_i is the initial concentration, C^* is the equilibrium concentration and r_0 is the radius of the spherical drop. Solution of Eq. (5.56) can be expressed as Eq. (5.57).

$$C=C^*+(C_i-C^*)\left[1-\frac{r_0}{r}\sum_{n=0}^{\infty}\left\{\text{erfc}\frac{(2n+1)r_0-r}{2\sqrt{D\theta}}\right.\right.$$

$$\left.\left.-\text{erfc}\frac{(2n+1)r_0+r}{2\sqrt{D\theta}}\right\}\right] \tag{5.57}$$

Now, we refer to the mean concentration of the drop as $\overline{C}$ which can be described as

$$\overline{C}=\int_0^{r_0} C(4\pi r^2)\,dr/(4/3)\pi r_0^3 \tag{5.58}$$

Substituting Eq. (5.57) into the right-hand side of Eq. (5.58), and then integrating we obtain

$$\overline{C}=C^*+(C_i-C^*)\left[1-3\tau\left\{(2/\sqrt{\pi})-\tau+4\sum_{n=1}^{\infty}\text{ierfc}(n/\tau)\right\}\right] \tag{5.59}$$

where $\tau\equiv\sqrt{D\theta}/r_0$ and $\text{ierfc}(x)=\int_0^x \text{erfc}(x)\,dx=(1/\sqrt{\pi})\exp(-x^2)-x\cdot\text{erfc}(x)$. When θ becomes sufficiently small, then $(n/\tau)\to\infty$, and thus it can be found that ierfc $(n/\tau)\to 0$.

Namely, when θ becomes small enough, we can describe Eq. (5.59) as

$$F=1-3\tau(2/\sqrt{\pi}-\tau) \tag{5.60}$$

where $F\equiv(\overline{C}-C^*)/(C_i-C^*)$.

Differetiating Eq. (5.60) with respect to τ, we obtain

$$\frac{dF}{d\tau}=-\frac{6}{\sqrt{\pi}}+6\tau \tag{5.61}$$

Furthermore, we have $(d^2F/d\tau^2)>0$; then, it can be found from Eq. (5.61) that the value of F becomes minimum at $\tau=1/\sqrt{\pi}$. Therefore, Eq. (5.60) is applicable over the range $0<\tau<(1/\sqrt{\pi})=0.564$.

Namely, we have a lower limit of r_0 at which Eq. (5.60) becomes applicable as follows:

$$r_0 = \sqrt{D\theta}/(0.564) \tag{5.62}$$

Sheridan[18] reported the empirical equation concerning the equilibrium concentration of hydrogen as follows:

$$\log C^* = -\frac{1600}{T} + 0.928 + \frac{1}{2}\log P_H \tag{5.63}$$

where P_H is the partial pressure of hydrogen in the vacuum tank. In Eq. (5.63), P_H, T and C^* have the units of Torr=mm Hg, K and ml/100 g, respectively. Thus, from Eq. (5.63), the value of C^* can be determined from the data of P_H and T. Therefore, when the data of r_0, θ, D, C_i and C^* are given, we can evaluate $\overline{C}$ from Eq. (5.60), as far as θ is sufficiently small. Moreover, we can find from the numerical computation that when the diameter of drop is less than 1 mm, the pressure in the vacuum tank which is required for degassing up to the designated $\overline{C}$ may be rather high.

Nomenclature

A : amplitude (−), cross-sectional area of up-leg (m^2)
a : interfacial area per unit volume of the ascending two-phase fluid (1/m)
C : concentration (kg/m^3), ($kmol/m^3$)
$C_{i,j}$: initial concentration of j-component (kmol(j)/kg(Fe))
C_j : conentration of j-component (kmol(j)/kg(Fe))
C^* : equilibrium concentration ($kmol/m^3$)
$\overline{C}$: mean concentration ($kmol/m^3$)
c_{gj} : concentration of j-component in a bubble ($kmol(j)/m^3$)
c_{lk}, c^i_{lk} : bulk and interface concentrations of k-component ($kmol(k)/m^3$)
D : diameter of vessel, diameter of bubble(m), molecular diffusivity (m^2/s)
D_u : inner diameter of up-leg (m)
d_{bo} : bubble diameter at nozzle tip (m)
d_n : nozzle diameter (m)
E_o : entrainment coefficient (−)
F_b : effective buoyancy force (N)
F_f : friction force (N)
F_g : gravitational force (N)
F_p : force due to pressure (N)
f : friction factor (−)
g : gravitational acceleration (m/s^2)
$g(s)$: transfer function (−)
H : liquid depth (m)
I : inverse of the mass transfer resistance (1/s)
K : equilibrium constant
k_{lk} : mass transfer coefficient of k-component (m/s)
M_g : mass flow rate for gas (kg/s)
M_j : molecular weight of j-component (kg(j)/kmol(j))
m : momentum rate ($m\cdot kg/s^2$)
N : number of tanks (−)

P_{co} : pressure of CO (Pa)
p_s : pressure at surface (Pa)
Q_{Feo} : production volume rate of FeO (kg/s)
Q_g : volumetric flow rate of rising bubble (m^3/s)
Q_l : liquid flow rate (m^3/s)
q : recirculation flow rate (m^3/s)
R : radius of vessel($D/2$) (m)
R : gas constant (J/kmol·K)
r : radius of plume (m), radial position in a drop (m)
r_o : radius of a spherical drop (m)
r_h : radius of plume at $Z=H-h$ (m)
s : feeding rate of available oxygen (kg(O)/s), operator of Laplace transformation (1/s)
T_g : gas temperature (K)
t_c : circulation time (s)
u_b : ascending velocity of a single bubble (m/s)
u_g : velocity of gas (m/s)
u_{gh} : velocity of gas at $Z=H-h$ (m/s)
u_l : velocity of liquid (m/s)
u_{lc} : mean velocity in the descending flow zone (m/s)
u_{lh} : velocity of liquid at $Z=H-h$
u_r : relative velocity of bubble to u_l (m/s)
u_s : slip velocity (m/s)
V : volume of liquid (m^3)
V_b : bubble volume (m^3)
V_{bo} : initial bubble volume (m^3)
w : metal volume (m^3)
Z_f : distance between gas injecting point and surface (m)
$Y(s)$: total transfer function (−)
Z : vertical distance from bottom or from blowing point (m)
ε : void fraction in two-phase flow (−)
θ : time (s)
ρ_g : density of gas (kg/m^3)
ρ_{gs} : density of gas at surface (kg/m^3)
ρ_l : density of liquid (kg/m^3)
σ^2 : variance (s^2)
σ_θ^2 : dimensionless variance (−)
ϕ : gas hold-up (−)
ϕ_h : gas hold-up at $Z=H-h$ (−)

References

1) Tamamoto, S., Ikeda, T. and Marukawa, K., Tetsu-to-Hagané, 54, 381 (1968).
2) Japan Society for the Promotion of Science, 19th Committee, Recommended Values of Equilibrium Constants for the Reaction in Steelmaking, 40, 2, 73, 112, Nikkan Kōgyo Shinbun, (1968).
3) Hsieh, Y., Watanabe, Y., Asai, S. and Muchi, I., Tetsu-to-Hagané, 69, 596 (1983).

4) Levenspiel, O., "Chemical Reaction Engineering", 2nd ed., 304, John Wiley & Sons, (1972).
5) Maruyama, T., Kamishima, N. and Mizushina, T., J. Chem. Eng. Japan, 17, 120 (1984).
6) Sahai, Y. and Guthrie, R. I. L., Met. Trans., 13B, 193 (1982).
7) Sahai, Y. and Guthrie, R. I. L., Met. Trans., 13B, 203 (1982).
8) He, Ji-C., Asai, S. and Muchi, I., Tetsu-to-Hagané, 70, 1590 (1984).
9) Davidson, J. F. and Harrison, D., Chem. Eng. Sci., 21, 731 (1966).
10) Davidson, L. and Amick, Jr, E. H., A. I. C*h*. E. Journal, 2. 337 (1956).
11) Fujii, T and Muchi, I., Tetsu-to-Hagané, 56, 1165 (1970).
12) Kato, Y., Kagaku Kōgaku, 26, 1068 (1962).
13) Govier, G. W., Radford, B. A. and Dunn, J. S., Can. J. Chem. Eng., 25, 59 (1957).
14) Stenning, A. H. and Martin, C. B., Trans. ASME, 90, 106 (1968).
15) Miyagawa, K., Nomura, E., Nozaki, Z., Adachi, T., Kishida, T. and Mori, K., Tetsu-to-Hagané, 53, 302 (1967).
16) Watanabe, S., Watanabe, H., Asano, K., Nakayama, M., Miyagawa, K. and Nomura, E., Tetsu-to-Hagané, 50, 1773 (1964).
17) Watanabe, H., Asano, K. and Saeki, T., Tetsu-to-Hagané, 54, 1327 (1968).
18) Sheridan, A. T., "Vacuum degassing of steel", Spec. Report No. 92, 53, The Iron and Steel Institute (1965).
19) Khang, S. J. and Levenspiel, O., Chem. Eng. Sci., 31, 569 (1976).